Spectroscopic model characterisation of hot exoplanet atmospheres

Elin Sandvik

Lund Observatory
Lund University

2022-EXA198

Degree project of 60 higher education
credits (for a degree of Master)

Supervisor: Jens Hoeijmakers

Lund Observatory
Box 43
SE-221 00 Lund
Sweden

Acknowledgements

First and foremost, I wish to express my gratitude to my supervisor, Jens Hoeijmakers. His expertise, support, and enthusiasm for the field is more than I could have ever wished for. I greatly appreciate all of his feedback and challenges, as they have made me develop a deep interest in exoplanet spectroscopy. I would also like to thank the examiner of my thesis, Thomas Bensby, for useful and constructive feedback. For their development of the analytical approximation on which I based my science question, I would like to thank Kevin Heng and Daniel Kitzmann for their work and feedback on my results. Furthermore, I would like to thank everyone in my research group for their continuous support and inclusivity. Working with you has been a joy. Lastly, I want to thank my family and friends for their love, encouragement, and moral support that I needed when running into obstacles during the project.

Popular science summary

The light emitted from a star can reveal details of its chemistry, formation, and evolution. It can also aid us in uncovering the exciting secrets of exoplanets, which we cannot directly observe. Since exoplanets are so small and dim compared to their host stars, we need sensitive instruments to distinguish between them. We find exoplanets through various detection methods. The transit method is most successful, followed by the radial velocity, gravitational microlensing, and direct imaging methods. We have discovered nearly 4000 exoplanets through the transit method, which is four times more than we have discovered through the radial velocity method.

A transit happens when an exoplanet passes before its host star, and a small fraction of the light gets blocked. An exoplanet is detected when these happen periodically and get confirmed by observations with other methods. However, the information from the transits also allows us to characterise exoplanets and uncover information regarding their atmospheric chemical composition. We can uncover these because starlight gets absorbed or scattered in the atmosphere. The imprint left on the stellar spectrum reveals details of the transiting exoplanet's chemical composition. The imprint is better known as transmission spectroscopy, where photons of different energies, or wavelengths, will have varying strengths depending on the atmosphere's chemical composition. Hot Jupiters are excellent targets for transmission spectroscopy due to their short orbital periods and giant puffy atmospheres with rich chemistry. They are also larger and hotter than other planets, making them easier to observe and characterise.

The information we receive from transmission spectroscopy must be analysed through models so we can characterise the exoplanet. Analysing the data is not a simple task since many parameters shape the appearance of the spectrum. Fast models and approximations are vital to interpreting these results. We must investigate different values of many parameters until we find the combination that best describes our transmission spectrum. The advantage of advanced models is that they include a comprehensive list of parameters that we can alter to represent the physical processes of the atmosphere accurately. However, the time it takes to fit a model to the data successfully can be too long due to the model's complexity. At this point, we need appropriate approximations to speed up the computations without a considerable loss of accuracy.

Approximations make analyses incredibly fast, though we sacrifice the wide range of physical parameters and lose reliability. However, there are instances where approximations do an incredible job at computing near-identical results to the complicated models. In these instances, using approximations is advisable as they are time-efficient. Unfortunately, a similar outcome between models and approximations is not always the case, and sometimes the solutions are vastly different. Therefore, we must quantify where we can reliably use the fast approximations without doubting their accuracy. Where and when we can confidently use these turns out to be a complicated matter, as will be investigated and explained further in this project.

Abstract

Hot Jupiters are gas giants under intense stellar radiation with short orbital periods of only a few days. Due to their large radii, hot temperatures, and large scale heights, hot Jupiters can be observationally characterised in detail through spectroscopy over an entire orbital phase. Transmission spectroscopy is one of the tools that aid us in understanding the complex chemistry of exoplanet atmospheres.

Observations are not the only method of estimating atmospheric compositions. For example, we can use advanced codes to model an exoplanet's chemical compositions and radiative transfer. However, advanced models are computationally expensive. When performing abundance retrievals where you have to create hundreds of thousands of model templates, we need approximations that are fast enough for retrieval algorithms.

In this project, we have used the semi-analytical code `FastChem` to model atmospheric chemical composition and `petitRADTRANS` to model the radiative transfer. From `petitRADTRANS`, we can model transmission spectra for different planetary parameters and choose whether we want a constant abundance throughout the atmosphere and whether we want to include variable gravity or not. We then wish to compare these solutions for different species with a fast analytical approximation. Heng & Kitzmann (2017) derived an analytical solution for the transit radius, which assumes an isothermal and isobaric atmosphere. They tested it for the WFC3 water band between 1.15-1.65 μm for a planet with a temperature of 1500 K. We wish to see whether it still holds for higher temperatures and other species.

The analysis has been performed for temperatures of 1500 K, 2500 K, and 3500 K, for the hot Jupiter HD 209458b. We have investigated H_2O, CO, Fe, Fe II, Ti, V, Mg, and Cr. These are interesting when studying ultra-hot Jupiters as they become detectable when the temperature is high. We found that the analytical approximation by Heng & Kitzmann (2017) works remarkably well for the species when the temperature is 1500 K. However, once we increase the temperature, we find that the approximation usually underestimates the spectral line strengths. For H_2O, it instead overestimates the spectral line strengths.

The analytical approximation by Heng & Kitzmann (2017) would benefit from including mass fractions, gravity, and mean molecular weight, which all vary with pressure and temperature for each atmospheric layer. However, the more we expand the approximation to improve its accuracy, the more computationally expensive it becomes. We need these fast models for retrieval algorithms, and there must be a balance between the approximation's accuracy and its computational speed.

We conclude that we must be careful when using the Heng & Kitzmann (2017) approximation and ensure that our application of the approximation is logical and within the scope of its capabilities. We must proceed with caution when analysing ultra-hot Jupiters, as the approximation's accuracy quickly deteriorates as we approach high temperatures. This is especially true for species such as Fe II that have a mass fraction that increases with altitude. Furthermore, we find that the approximation does poorly to varying degrees for different species. Therefore, it should not be used to perform relative abundance retrievals, especially for ultra-hot Jupiters.

Contents

1 Introduction **2**

2 Theory **9**
2.1 Analytical approximation of transit radius 9
2.1.1 Order-of-magnitude expressions 9
2.1.2 Isothermal atmospheres 10
2.2 Numerical methods for radiative transfer 14
2.3 Chemical equilibrium 14

3 Method **16**
3.1 `petitRADTRANS` 16
3.2 `FastChem` 18
3.3 Linking the codes 22
3.4 Error estimation 23

4 Results **24**
4.1 Analytical approximation & `petitRADTRANS` 24
4.1.1 Including variable mass fractions 27
4.1.2 Including variable mass fractions & variable gravity 29
4.1.3 Comparing correlation for different temperatures 31
4.1.4 Low-resolution 34
4.1.5 Varying the constant abundance 36
4.2 CO & Fe 38
4.3 Fe II 42
4.4 Ti, V, Mg, & Cr 44

5 Conclusions **52**
5.1 Future prospects 53

Chapter 1

Introduction

Almost 30 years ago, the discovery of small planets orbiting a pulsar (Wolszczan & Frail 1992), followed by the detection of the Jupiter-mass planet 51 Peg b (Mayor & Queloz 1995), sparked the discovery of thousands of exoplanets to follow. Exoplanet research is a multi-disciplinary science, where astronomy, astrobiology, geology, chemistry, biology, astrophysics, and planetary science are some of the fields that collaborate to understand the complete picture (Howell 2020). Many ponder whether we are alone in the Universe and whether other planetary systems can host life. Furthermore, we wish to understand our solar system and the planets orbiting the Sun and, most importantly, the Earth.

The transit method is one of the most popular methods to discover exoplanets. Some other methods of exoplanet discovery are the radial velocity method, direct imaging, and microlensing, though these will not be explained in this thesis. When observing the light from a star with the transit method, a dip in the flux will appear when an exoplanet intersects our line-of-sight (see Figure 1.1). The transit reoccurs periodically so that we can determine the orbital period of the exoplanet. The depth of the dip in the flux can also put constraints on the exoplanet's radius relative to its host star. However, the exoplanet's orbit needs to be aligned with our line-of-sight to be detected as it passes in front of its host star. For example, a typical hot Jupiter with a semi-major axis of 0.05 AU has a transit probability of $\sim$10%, while an Earth-like planet at 1 AU is as low as $\sim$0.5% (Deeg & Alonso 2018).

Unfortunately, the chance of "false positives" for transits is relatively high, which are signals that resemble planetary transits but could be grazing eclipses of a binary star (Winn 2014). Follow-up investigations are therefore necessary for confirmation. We primarily look at the shape of the light curve to determine whether it is an exoplanet or a binary star. If there is a grazing eclipse, the smaller transiting star will produce a more significant drop in brightness. Even though both stars emit light, the transiting star still blocks out a large portion of the light from the other star. An exoplanet would produce a much smaller drop in brightness since it is tiny compared to the host star. Furthermore, an exoplanet transit would result in a faster decline in brightness (Deljookorani et al. 2020).

Detecting exoplanets is not the only thing the transit method is useful for. By observing how the light emitted from a star changes when an exoplanet intersects our line-of-sight

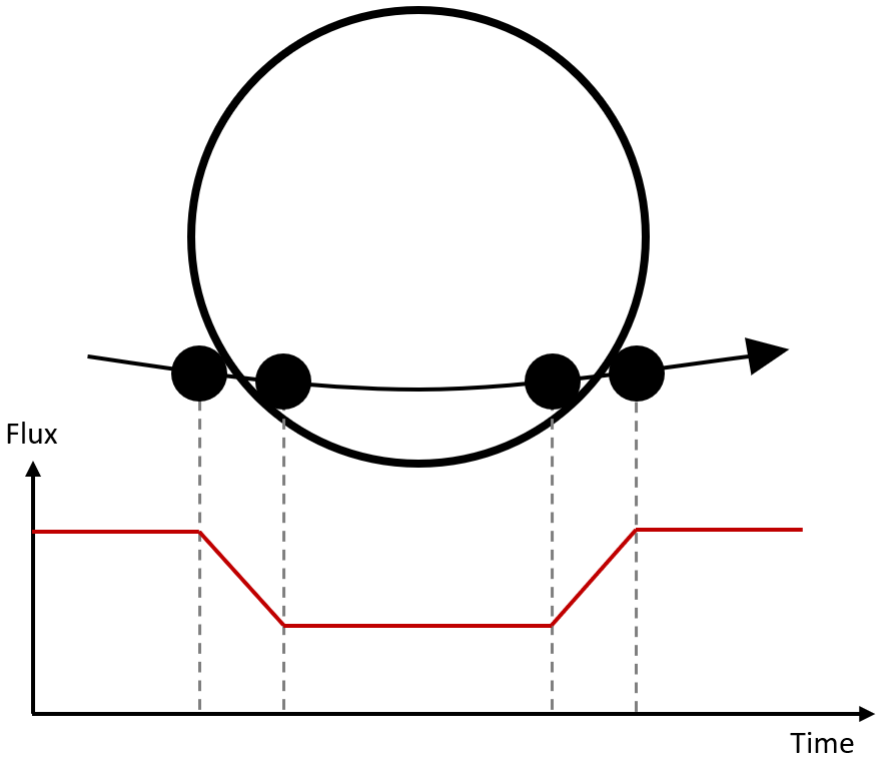

Figure 1.1: Illustration of an exoplanet transiting the star and how the flux changes.

with the host star, we can uncover details of the atmospheric composition. As the photons pass through the exoplanet atmosphere, they get absorbed and scattered. The imprints of the planet's atmospheric absorption will only leave small features on the stellar spectrum during the transit since the projection of the transit chord onto the stellar photosphere (see Figure 1.2) is very small. The transit chord is the projected path of the transiting exoplanet across the stellar disc (Boley et al. 2020). Each ray passes through the transit chord with varying degrees of transparancy or opaqueness. By summing up the contributions from all the chords, we can calculate the effective occulting area of an exoplanet at a given wavelength (Heng & Kitzmann 2017). We can see the imprints of atmospheric absorption when comparing the stellar spectrum to the spectrum during transit. Overlapping spectral lines between a star and planet for different species make it complex to confirm their detection and quantify their abundances. Furthermore, different wavelength regimes require instruments of varying resolution or specifications to detect the presence and abundance of certain species.

With the help of large-scale collaborations to construct telescopes capable of exoplanet detection and characterisation (such as the NASA Kepler mission (Borucki et al. 2010), TESS (Ricker et al. 2016), and CHEOPS (Cessa 2019)), we have observed a great variety of exoplanets, ranging from gas giants much more massive than Jupiter, intermediate-mass Neptune-like planets, and Earth-like terrestrial planets (Spiegel et al. 2014). Figure 1.3

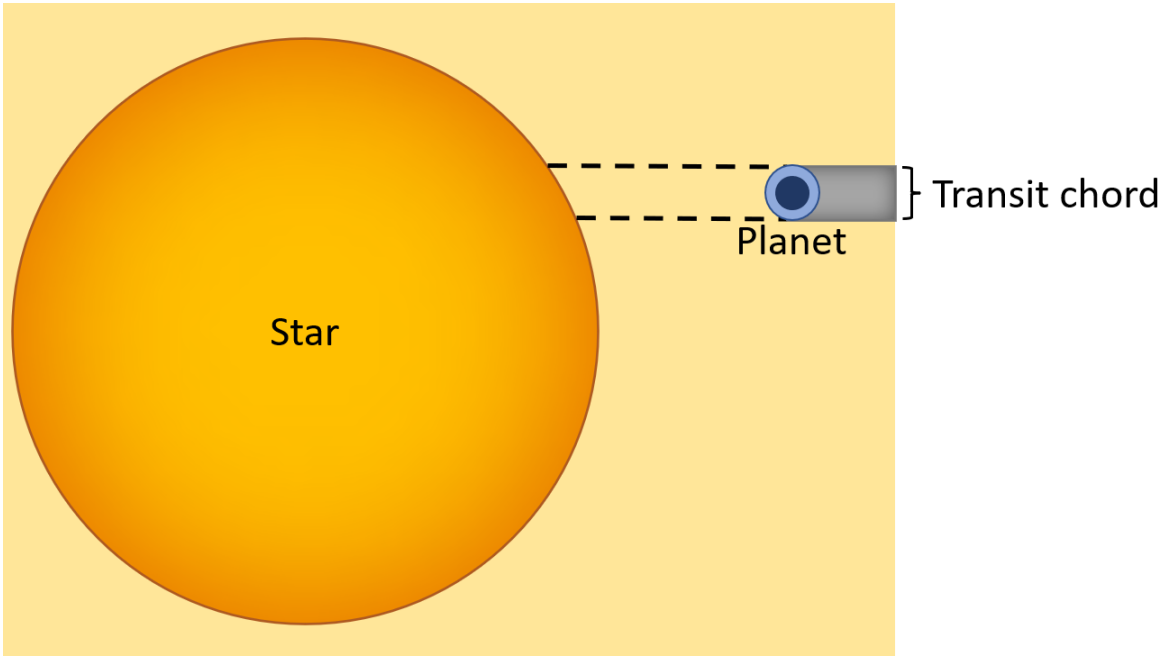

Figure 1.2: Illustration of a transit chord.

shows the distribution of exoplanets discovered with and without Kepler and how they were detected. For the search for life, small Earth and super-Earth-size rocky planets orbiting within their star's habitable zone are most interesting (Howell 2020). However, the other types of exoplanets are of interest since we want a broad understanding of the spectrum planets can occupy and how the parameters vary depending on the overall structure of their planetary system. In this project, we are mainly interested in the atmospheres of hot Jupiters and ultra-hot Jupiters around bright host stars.

Hot Jupiters are gas giants which orbit their host stars with typical orbital periods of only a few days. These planets are under intense stellar irradiation, which causes their unique thermal, chemical, and dynamical regime. Due to their large radii and hot temperatures, hot Jupiters can be observationally characterised in detail with spectroscopic observations over an entire orbital phase (Fortney et al. 2021). Gas giants have no well-defined surface, making their silhouettes fuzzy. As the host star irradiates the less opaque outer part of the atmosphere, only a tiny portion of the photons will be absorbed. This absorption is wavelength-dependent due to molecular and atomic scattering properties. For a strong transition which releases high-energy photons, the effective size of a planet's silhouette grows by a few atmospheric scale heights, which grows linearly with temperature. Thus, hot Jupiters' high temperatures yield stronger signals since they have larger scale heights. Strong atomic or molecular transition wavelengths result in a more opaque atmosphere, yielding a larger effective silhouette for the planet. The larger effective silhouette blocks us from seeing the planet's surface if its atmosphere is opaque at a certain altitude. We can thus gain knowledge of the atmospheric composition through the transmission

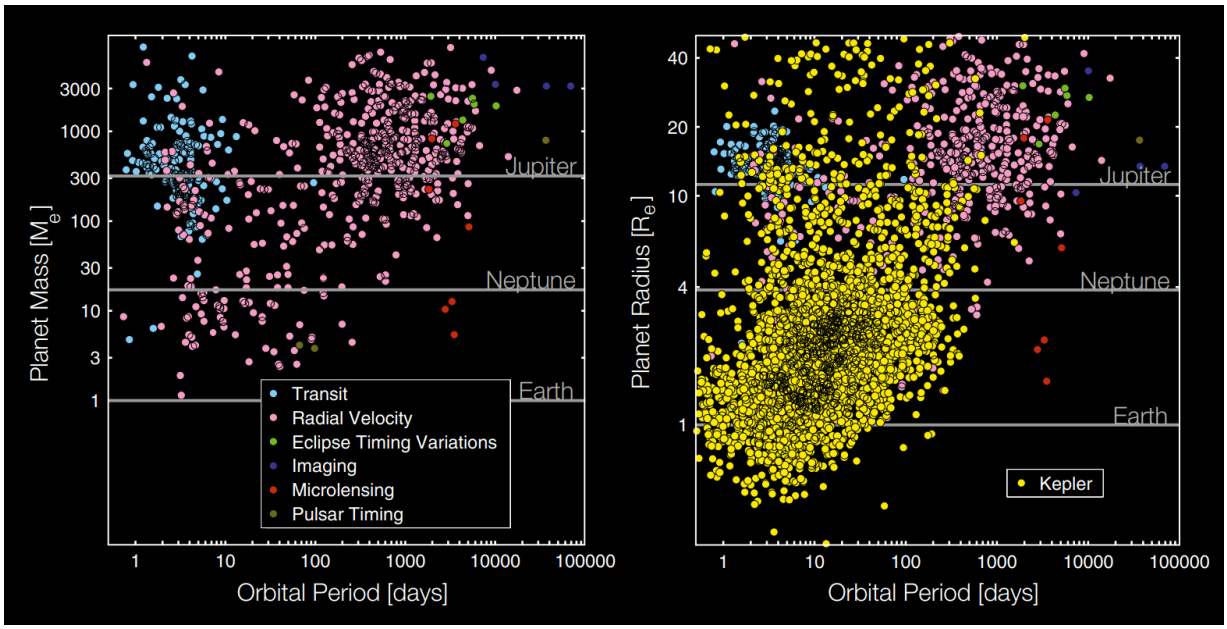

Figure 1.3: Confirmed exoplanets and their method of detection. The left figure shows those observed with instruments other than Kepler, and the right figure shows the inclusion of exoplanets discovered with Kepler (Batalha 2014).

spectrum (Winn 2014).

After all, one of the most crucial aspects of understanding exoplanets and planetary systems is understanding their atmospheres' chemistry and radiative properties. Each planet has its complex chemistry, even in our solar system. Although it is far more challenging to understand the properties of exoplanet atmospheres than those in our solar system, we have modern tools that make it possible to scratch the surface of their complexity. Transmission spectroscopy is one of the tools that aid us in understanding the chemistry of exoplanet atmospheres.

The Hubble Space Telescope (HST) wields the Wide Field Camera 3 (WFC3) which sits atop the water band in near-IR from 1.1 to 1.7 μm, and has allowed for the detection of water vapour in exoplanet atmospheres (Deming et al. 2013a). However, its full range includes direct, high-resolution imaging from 200 to 1700 nm. The large wavelength range, combined with its high sensitivity, high spatial resolution, large field of view, and wide selection of spectral elements, makes the WFC3 a versatile instrument (Dressel 2021). In addition, ground-based telescopes are also used, e.g. ESPRESSO on the VLT, covering a spectral range of 380 to 788 nm (Pepe et al. 2021), and HARPS on the ESO 3.6-metre telescope with a spectral range of 378 to 691 nm (Mayor et al. 2003).

WFC3 offers low-resolution spectroscopy over a wide range of wavelengths, whereas ESPRESSO and HARPS provide high-resolution for a narrower range covering the optical and near-IR regimes. These are complementary since multiple species can overlap and create difficulties in molecular identification and abundance determinations for low-resolution

spectroscopy (Brogi et al. 2017). On the other hand, it is challenging to retrieve atmospheric properties and absolute molecular abundances from high-resolution. This is partly due to the loss of the planet and star continuum from self-calibration of data, and also due to the lack of robust retrieval algorithms (Brogi et al. 2017). Combining high-resolution and low-resolution data yields tight constraints on the chemical compositions of a planet's atmosphere (see Brogi et al. 2017 for details).

Observations are not the only way to estimate atmospheric compositions. Plenty of models have developed over the years, such as analytical formulas or intricate codes. In this project, the codes `FastChem` (Stock et al. 2018) and `petitRADTRANS` (Mollière et al. 2019, 2020; Alei et al. in prep.) have been used to produce transmission spectra of exoplanet atmospheres with varying chemical abundances depending on the pressure in the atmosphere. `FastChem` is a semi-analytical code that computes the chemical composition of an atmosphere from simple parameters, whereas `petitRADTRANS` computes the radiative transfer. The latter needs atmospheric chemistry to produce spectra, so we wish to create a link from `FastChem` to `petitRADTRANS` to prescribe the chemical composition.

Specifically, we have looked at transmission spectra in this project. Other high-resolution transmission spectroscopy studies have found that hot and ultra-hot Jupiters have atmospheres rich in a broad range of atomic and ionized metallic species and molecules (Fortney et al. 2021). Furthermore, studies have developed a deeper understanding of atmospheric dynamics since one can assess the velocity and direction of atmospheric flow using the Doppler shifts of absorption lines (Flowers et al. 2019). To interpret data from transmission spectroscopy, we typically assume 1D cloud-free atmospheres in chemical equilibrium, though more advanced 3D and non-chemical equilibrium models are likely more accurate. These assumptions may be more or less appropriate depending on the planet's temperature. However, they are necessary since typical observations have not yet reached the point where they are informative enough to allow us to add additional complexity. Furthermore, simple models are less computationally expensive, which is necessary for them to be fast enough for retrieval algorithms.

Although observations and data are constantly produced, reliable numerical and analytical models are necessary if we wish to analyse these. Models are an essential tool in science, as they allow scientists to answer science questions and interpret data. They also inform them of what is possible to look for during observations or experiments. We will use the numerical tools `FastChem` and `petitRADTRANS` to model atmospheric chemistry and radiative transfer to produce transmission spectra. We also want to compare the numerical results of `petitRADTRANS` to an analytical solution. Heng & Kitzmann (2017) derived an analytical approximation for computing the transmission spectrum of an exoplanet atmosphere, where expressions for both isothermal and non-isothermal atmospheres are available. To analyse the data, we must typically create hundreds of thousands of model templates. Advanced solutions by numerical models can take several minutes to produce a single model, whereas an analytical approximation only takes a second at most. The simpler and faster route is preferable if an analytical approximation can reproduce the same results as more complicated algorithms.

Isothermal temperature structures are a simple way to model atmospheres, though it

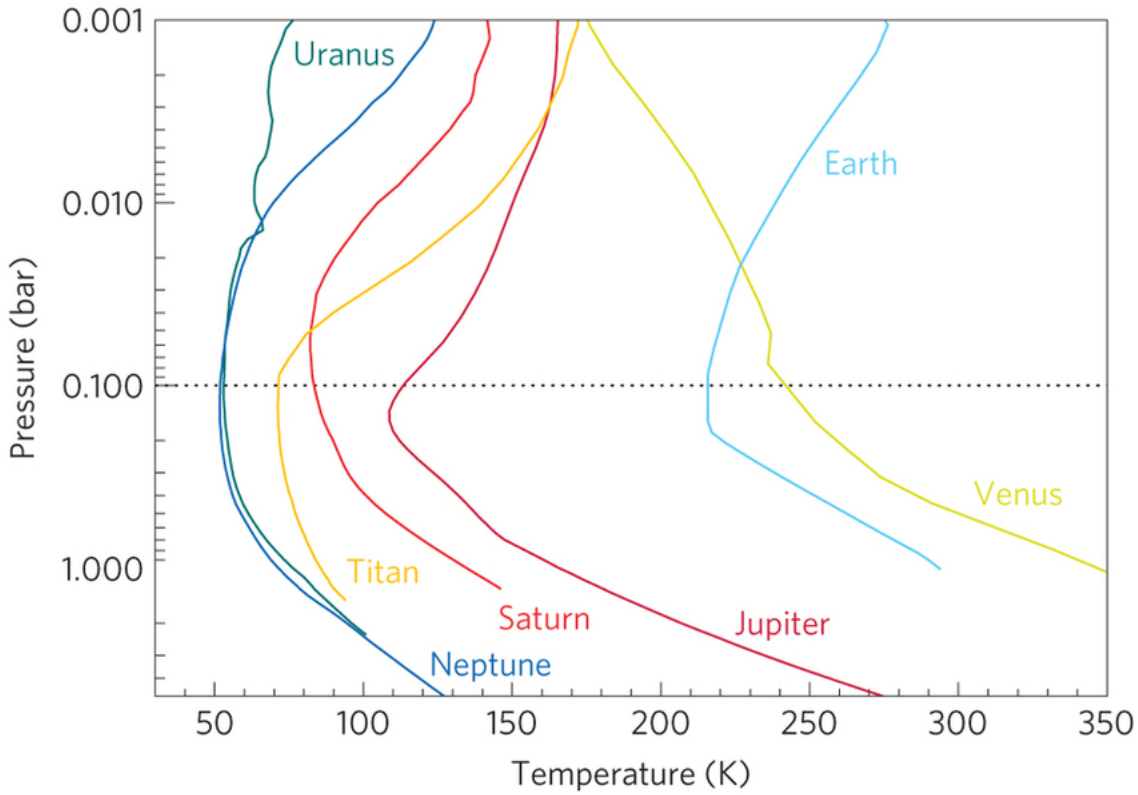

Figure 1.4: Temperature-pressure profiles for bodies with thick atmospheres in the solar system (Robinson & Catling 2013).

is an approximation and is not true to the structures we typically see. An example of the temperature-pressure (T-P) profile for objects in the solar system with thick enough atmospheres is seen in Figure 1.4. However, T-P profiles are complex. If we want realistic models, we need to account for the optical depth, atmospheric opacity in infrared (IR), atmospheric equilibrium temperature, and internal planetary temperature (Guillot 2010).

The scientific question for this project is to which degree this analytical approximation for isothermal atmospheres correlates with transmission spectra produced by `petitRADTRANS` and to quantify the differences between the two. The study will also highlight the importance of parameters such as varying chemical abundances and variable gravity. These may be disabled in `petitRADTRANS` and we will investigate their effect on the results as we add more complexity to our model. This is of interest since many have used the analytical approximation to retrieve abundances from their spectra (Gibson et al. 2020; Gibson et al. 2022). We will investigate if the method may do a poor job in certain regimes for some species, at different temperatures. Heng & Kitzmann (2017) produced results in low-resolution for the water band between 1.15 μm to 1.65 μm of a hot Jupiter, which proved successful. We wish to examine whether this still holds for high-resolution, high temperature, and other species. Gibson et al. (2020) and Gibson et al. (2022) applied the analytical approximation to analyse the spectrum of an ultra-hot Jupiter. However,

the approximation was not benchmarked for such high temperatures and we cannot assume that it will hold. A transmission spectrum is heavily influenced as we increase the temperature to extreme values, which is the case for ultra-hot Jupiters.

Suppose the analytical formula yields similar results to the solution by `petitRADTRANS` with the inclusion of chemistry from `FastChem` and variable gravity. In that case, it might be a simpler and less computationally expensive method to compute transmission spectra. If it does not yield accurate results for high temperatures or certain species, we cannot use it to create model templates and draw accurate conclusions of the exoplanet's atmosphere from our data. We must establish which species and temperatures the analytical approximation holds for and what to be wary of when using it. Finally, from the results we can draw conclusions regarding which aspects of the analytical approximation are most important to improve upon, if we wish to create a more accurate, but still fast, approximation.

Chapter 2

Theory

2.1 Analytical approximation of transit radius

We wish to understand how valid the analytical approximation of a transit radius is, as Heng & Kitzmann (2017) (HK17) derived. We will proceed to build an analytical description of the transmission spectrum, and the first purpose of this project is to verify its accuracy. We will reproduce a figure from HK17, which tests the approximation on the molecular water band between 1.15-1.65 μm.

We follow the steps of HK17 and model an atmosphere with a constant number density n which only contains a single molecule with extinction cross-section σ is isothermal, i.e. we can describe the whole atmosphere with a single temperature T. We then define the pressure scale-height as

$$H = \frac{kT}{mg}, \tag{2.1}$$

where k is the Boltzmann constant, m is the mass of said molecule, and g is the surface gravity.

2.1.1 Order-of-magnitude expressions

H is expected to be much smaller than the transit radius R, such that the characteristic length scale of the system is the geometric mean of the two as $\sqrt{HR}$. We can then simplify the chord optical depth as

$$\tau \sim n\sigma\sqrt{HR} \sim 1. \tag{2.2}$$

Using the ideal gas law, we can rearrange the above expression for the transit radius R in terms of the opacity κ

$$R \sim H\left(\frac{g}{P\kappa}\right)^2, \tag{2.3}$$

where P is the pressure. The opacity function κ is dependent on chemical composition and thus the mixing ratios, which can be computed with `FastChem`. For this reason, we later wish to compute the chemistry with `FastChem` first, use it to produce transmission spectra with `petitRADTRANS`, and finally compare it to the analytical approximation.

2.1.2 Isothermal atmospheres

We now consider an observer who records a transit radius of R' and define a radial coordinate r', where $r' = 0$ is located at R'. The radial coordinate is then dependent on the spatial coordinate x of the observer's line-of-sight, such that $r' \approx x^2/2R'$. The number density n of an isothermal atmosphere is then dependent on n', which is the number density at R', yielding $n = n' \exp(-r'/H)$. Assuming that σ is spatially independent, we can evaluate the integral $\int_{-\infty}^{+\infty} n\sigma \, dx$ and obtain

$$\tau = n'\sigma\sqrt{2\pi H R'}. \tag{2.4}$$

As we can see, the expression in equation 2.2 lacks a factor of $\sqrt{2\pi}$. The characteristic length scale $\sqrt{2\pi H R'}$ only appears if the integration is performed from $-\infty$ to $+\infty$.

We now redefine the coordinate system with the radial coordinate r such that $r = 0$ is located at the centre of the exoplanet. Now $r' = 0$ sits at $r = R_0$, which is the reference transit radius. At this point, we also have the reference pressure P_0 and number density n_0. Since we cannot see the surfaces of hot Jupiters and ultra-hot Jupiters due to their enormous atmospheres, we set the reference transit radius R_0 to be the planetary radius and the reference surface pressure P_0 is chosen at the same point. An illustration of the coordinate system's geometry can be seen in Figure 2.1. It then follows that n' (which is the same as in the previous paragraph) is $n' = n_0 \exp[-(r - R_0)/H]$, and the chord optical depth is approximately

$$\tau = \tau_0 \exp\left(-\frac{r - R_0}{H}\right), \tag{2.5}$$

since $R' = R_0 + r' \approx R_0$ and we can therefore approximate that the transit radius is equal to the reference transit radius. The reference optical depth (which is associated with a reference pressure where the atmospheric layer may or may not be chosen to be optically thick) is then

$$\tau_0 = \frac{P_0\sigma}{kT}\sqrt{2\pi H R_0}, \tag{2.6}$$

from which we can derive a relation between τ and r, since τ_0 is independent of r. We differentiate equation 2.5 w.r.t. r such that

$$\begin{aligned}\frac{d\tau}{dr} &= \frac{d}{dr}\left(\tau_0 \exp\left(-\frac{r - R_0}{H}\right)\right) \\ &= -\frac{1}{H}\underbrace{\tau_0 \exp\left(-\frac{r - R_0}{H}\right)}_{\tau}.\end{aligned}$$

By rearranging the above expression, we find that

$$dr = -\frac{H d\tau}{\tau}. \tag{2.7}$$

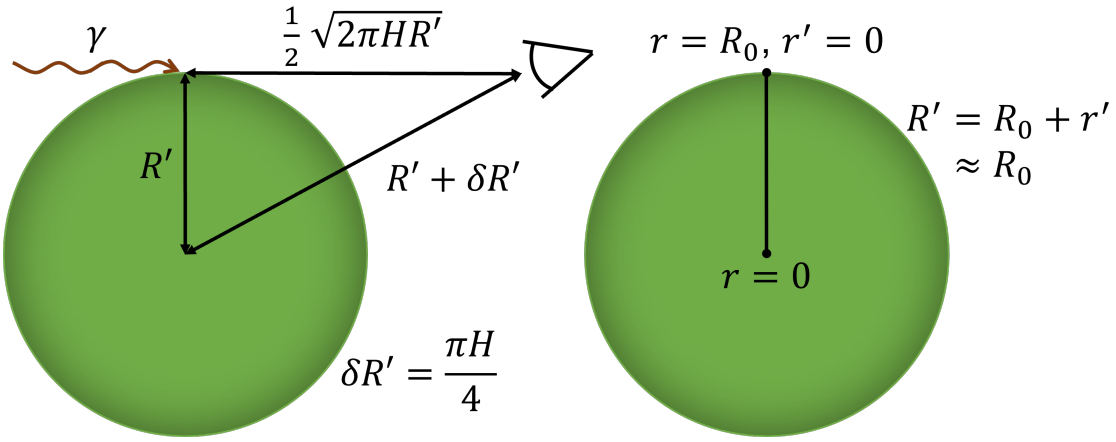

Figure 2.1: An illustration of the geometry of the coordinate system used to derive HK17's analytical approximation.

The effective thickness of the atmosphere at a given wavelength is h, such that the transit radius is $R = R_0 + h$. The projected size can be expressed as either πR^2 or $\pi R_0^2 + A$, where A is the area of the annulus above the reference radius

$$A = 2\pi \int_{R_0}^{+\infty} [1 - \exp(-\tau)] r \, dr. \tag{2.8}$$

Since we expect that A is typically much smaller than πR_0^2, the effective thickness of the atmosphere is

$$h = \frac{A}{2\pi R_0}. \tag{2.9}$$

Changing coordinate from r to τ yields

$$h = H \int_0^{\tau_0} \left(\frac{1 - \exp(-\tau)}{\tau} \right) \left[1 + \frac{H}{R_0} \ln \left(\frac{\tau_0}{\tau} \right) \right] d\tau. \tag{2.10}$$

The term H/R_0 may be neglected since it is much smaller than the other term. As proposed in HK17, we use the identity in equation (10) of Appendix I of Chandrasekhar (1960)

$$E_1 = -\gamma - \ln \tau_0 + \int_0^{\tau_0} \frac{1 - \exp(-\tau)}{\tau} \, d\tau, \tag{2.11}$$

where $\gamma \approx 0.57721$ is the Euler-Mascheroni constant. The E_1 quantity is the exponential integral of the first order with the argument τ_0. As $\tau \to \infty$, we have that $E_1 \to 0$, which yields

$$h = H(\gamma + \ln \tau_0 + E_1). \tag{2.12}$$

Generally, we expect the atmosphere to be optically thick at the reference transit radius, such that $\tau_0 \gg 1$. The E_1 term vanishes if such is the case, and yields that the effective

chord optical depth associated with the transit radius R is

$$\tau_{\text{eff}} = \tau_0 \exp\left(-\frac{h}{H}\right) = \exp(-\gamma) \approx 0.56. \tag{2.13}$$

This leads us to the expression for the transit radius, assuming an isothermal atmosphere, to be

$$R = R_0 + H\left[\gamma + \ln\left(\frac{P_0\kappa}{g}\sqrt{\frac{2\pi R_0}{H}}\right)\right]. \tag{2.14}$$

As noted in HK17, the transit radius is linearly dependent on H and is a slowly varying function of κ. Opacity generally varies over many orders of magnitude, and therefore its effect on the transmission spectrum is comparable to the pressure scale height.

They modelled the transmission spectrum of HD 209458b (see Table 4.1 for parameters), as seen in Figure 2.2. Initially using a spectral resolution of $\Delta\lambda \sim 0.01$ nm, they binned the result down to ~ 1.0 nm and ~ 0.1 nm to illustrate minor discrepancies between their work and the work of Deming et al. (2013b), Fortney et al. (2010), and Line et al. (2013).

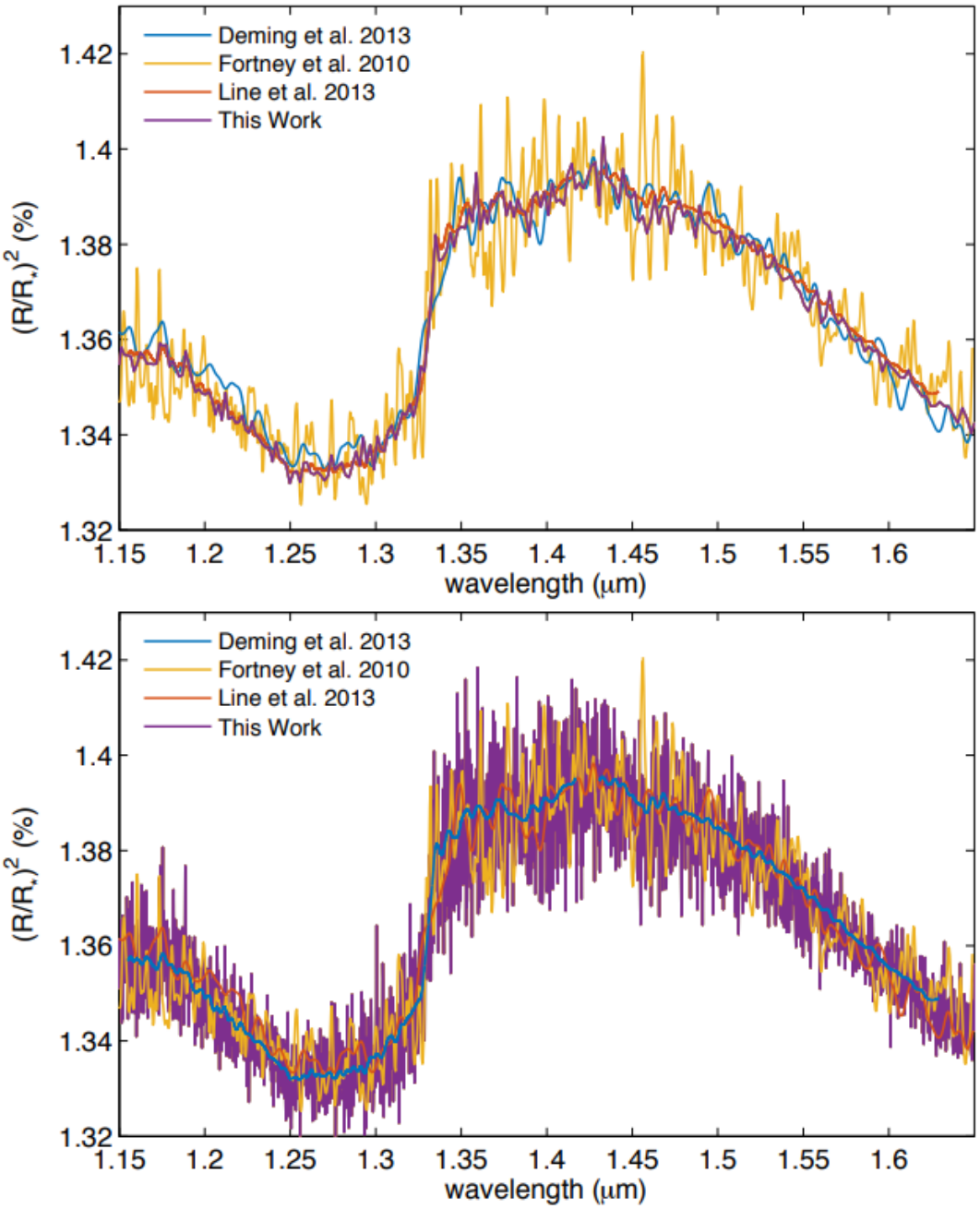

Figure 2.2: Transmission spectrum of HD 209458b (see Table 4.1 for exact parameters) reproduced from HK17, where they compared their work to that of Deming et al. (2013b), Fortney et al. (2010), and Line et al. (2013). HK17 used a spectral resolution of $\Delta\lambda \sim 0.01$ nm which they binned down to ~ 1.0 nm and ~ 0.1 nm, respectively, to illustrate minor discrepancies.

2.2 Numerical methods for radiative transfer

What algorithms for radiative transfer essentially aim to evaluate is equation 2.5. This calculation takes place on a grid, typically in 1D, where the parameters are the local pressure, temperature, and composition. These together prescribe values for τ. Opacity functions are typically pre-computed and tabulated, derived from line-list measurements and models. These tools allow for prescriptions of chemical compositions, and a common approximation is that of chemical equilibrium.

2.3 Chemical equilibrium

The chemical composition in gas-phase is of great importance in planetary science, and in astrophysics in general. It impacts the hydrodynamic and thermodynamic structure of atmospheres - both planetary and stellar - but it also influences the spectral appearance of the object. In addition, the corresponding radiative transport coefficients of absorption, spontaneous, and induced emissions are affected. Furthermore, the atomic and molecular species build solid state bodies ranging from dust particles to rocky planets (Stock et al. 2018).

Chemical equilibrium occurs if the chemical time-scale is much shorter than the dynamical time-scale and if photochemical- and cosmic-ray-induced processes can be neglected (Stock et al. 2018). In this state, both reactants and products do not tend to change with respect to time, and the chemical properties of the system stay constant since the chemical time-scale is greater than the dynamical time-scale, which is defined as

$$\tau_{\mathrm{dyn}} = \sqrt{\frac{R^3}{2GM}}, \tag{2.15}$$

where R is the radius, G is the gravitational constant, and M is the mass. The dynamical time-scale is also known as the time it takes for an object to respond to deviations from the hydrostatic equilibrium, which is the balance between pressure and gravitational forces.

Chemical equilibrium thus means that forward and backward processes occur at the same rate such that the concentrations stay the same (Atkins & De Paula 2006). For an illustration of this, see Figure 2.3.

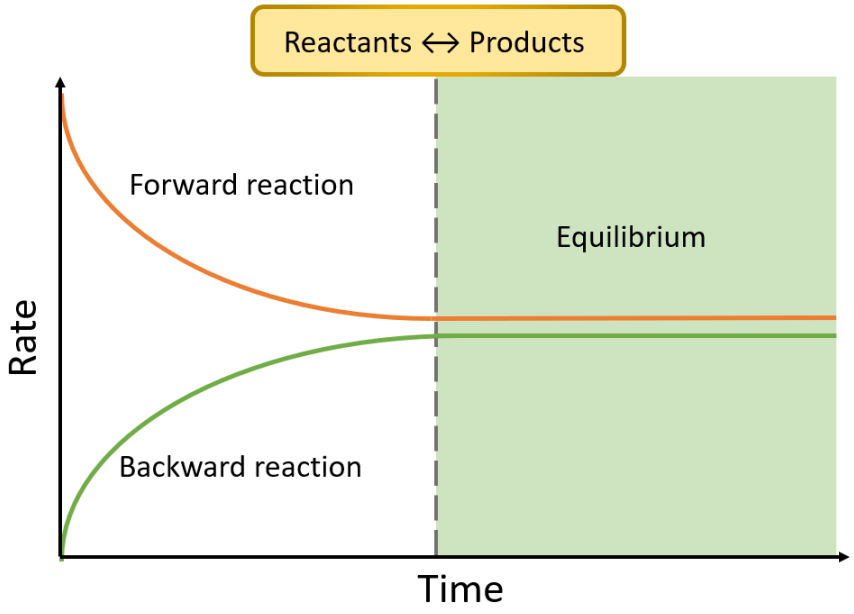

Figure 2.3: An illustration of chemical equilibrium, where the forward and backward processes occur at the same rate, reaching a point where the concentrations stay the same.

Chapter 3

Method

3.1 petitRADTRANS

The Python package petitRADTRANS (Mollière et al. 2019, 2020; Alei et al. in prep.) models radiative transfer in an exoplanet atmosphere and can be used to calculate emission and transmission spectra for clear and cloudy planets. Though it is possible to include a non-isothermal atmosphere in petitRADTRANS, we have focused on isothermal atmospheres.

petitRADTRANS assumes hydrostatic equilibrium and can compute both high-resolution and low-resolution spectra. High-resolution spectra run computations at $R = \lambda/\Delta\lambda \leq 10^6$, whereas low-resolution run for $R \leq 1000$. Examples of these can be seen in Figure 3.1, where the planet GJ 1132 b has been modelled using parameters from Swain et al. (2021). Several parameters must be known for the computations to proceed, such as surface gravity, temperature, planetary radius, mass fractions of species, surface pressure, and mean molecular weight. For GJ 1132 b, these are stated in Table 3.1 and Table 3.2. We also need opacity functions for line absorbers. These are retrieved from the DACE database (Grimm et al. 2021).

Table 3.1: The mass fractions for GJ 1132 b by Swain et al. (2021).

Mass fractions for GJ 1132 b				
H_2	He	CH_4	HCN	C_2H_2
0.3996	0.0009	0.0106	0.0179	0.0034
CO	CO_2	H_2O	N_2	NH_3
0.0185	5.6×10^{-10}	2.1×10^{-6}	0.5492	3.8×10^{-5}

Table 3.2: The parameters for GJ 1132 b by Swain et al. (2021), where T is the temperature, R_s is the host star's radius, R_p is the planetary radius, g_0 is the surface gravity, P_0 is the surface pressure at R_p, and MMW is the mean molecular weight.

Parameters of GJ 1132 b					
T [K]	R_s [$R_\odot$]	R_p [$R_\oplus$]	g_0 [cm/s^2]	P_0 [bar]	MMW
529	0.2105	1.15	1202.3	1.0	4.54

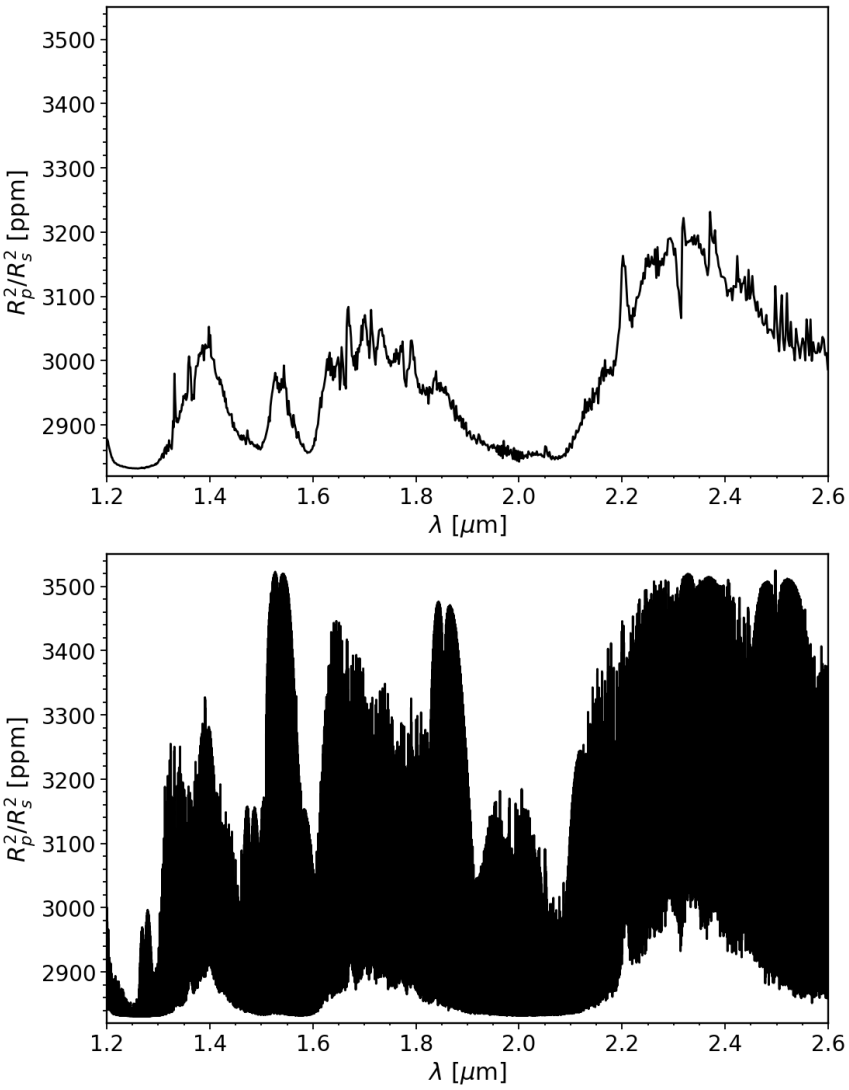

Figure 3.1: The two figures show the transmission spectrum of the same exoplanet, but the top figure shows a low-resolution case, and the bottom one shows a high-resolution case. Both are modelled with `petitRADTRANS`, with the parameters shown in Table 3.2 and 3.1. The most prominent features stem from CH_4 and smaller ones from HCN and C_2H_2.

3.2 FastChem

FastChem is a semi-analytical code which computes the chemistry of exoplanet atmospheres developed by Stock et al. (2018). The algorithm needs a list of chemical elements, molecules and ions as input. It also needs initial abundances of species, which are solar abundances adopted from Asplund et al. (2009) and altered manually whenever we wish to run computations for a different metallicity. The abundances are in logarithmic form, so if we wish to use a metallicity ten times greater than solar, we simply increase the value of each species' abundance by 1.

First, initial values of the electron density $n_0^{(0)}$ and correction terms $n_{j,\min}^{(0)}$ are set. The electrons are treated as chemical species in the algorithm. The logarithmic mass action constants $\ln K_i$ are calculated for a given temperature. Next, the number densities are calculated for all atomic species. We use these results to calculate the number densities of the molecular species through the law of mass action:

$$n_i = K_i \prod_{j \in \mathcal{E}_0} n_j^{\nu_{ij}} \qquad \forall i \in \mathcal{S} \setminus \mathcal{E}, \tag{3.1}$$

where $\mathcal{S}$ is the set of all chemical species in the gas phase (expect for the electron), $\mathcal{E}$ is the set of atomic species, and $\mathcal{E}_0$ is the set of atomic species with the electron included. We exclude the atomic species since we only wish to calculate the molecular species' number densities. The term ν_{ij} represents the coefficients of the stoichiometric matrix, which yields information about reactants and products in model reactions. Through these coefficients, we can calculate the number density of molecular species from the number densities of atomic species. The correction term $n_{j,\min}$ is then updated, and electron density n_0 is calculated. The process is then repeated (except for setting initial values) until a convergence criterion

$$\left| n_i^{(k)} - n_i^{(k-1)} \right| < \delta \left| n_i^{(k)} \right| \qquad \delta > 0 \tag{3.2}$$

has been met for all species $i \in \mathcal{S}$, where k denotes the iteration.

The output is a data file with the volume mixing ratio (VMR) of over 500 species at a given pressure and temperature. Examples of the outputs can be seen in Figure 3.2, where we have modelled the significance of the C/O ratio and its effect on the overall chemistry. In Figures 3.3-3.4, we have modelled the chemistry of Ti-bearing and V-bearing species for equilibrium temperatures of 2000 K and 3000 K. Figure 3.3 ran computations for solar metallicity, and Figure 3.4 for twenty times greater than solar metallicity.

The appearance of exoplanet spectra changes as the C/O ratio varies. High C/O ratios (>1.0) result in atmospheres rich in methane (CH_4), HCN, and hydrocarbons. A low (<0.8) C/O ratio leads to an oxide-rich atmosphere, with H_2O as well as TiO and VO (Kitzmann et al. 2018). Hot Jupiters with $T_{\rm eq} > 2000$ K have been postulated to contain TiO and VO in gaseous form, which strongly absorb UV and visible light. The absorption would heat the upper atmosphere, leading to a rise in temperature with altitude and thus resulting in a thermal inversion (Merritt, S. R. et al. 2020). The C/O ratio and TiO abundance are strongly correlated, as a higher C/O ratio would lead to the depletion of TiO. This can be

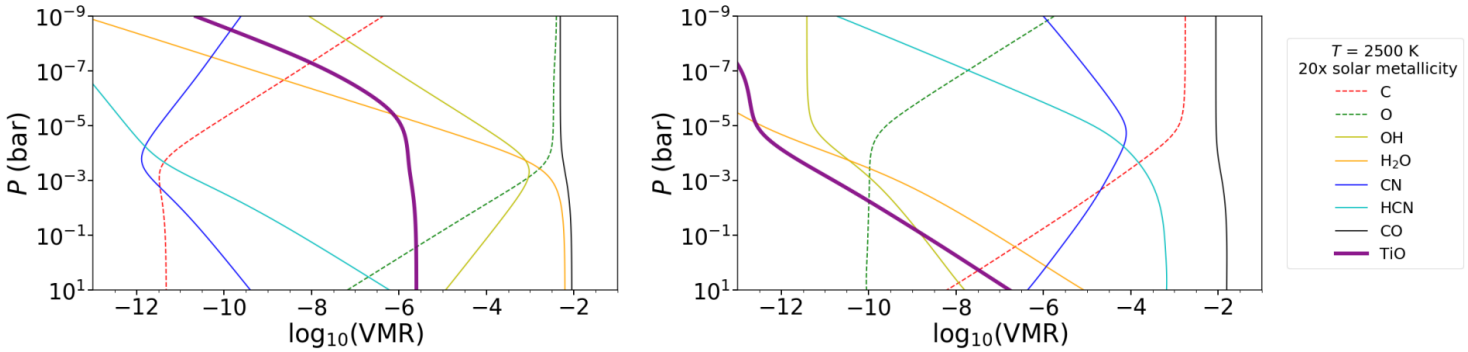

Figure 3.2: Comparison between solar C/O ratio of 0.55 (left) and C/O ratio of 1.2 (right). In the latter case, the carbon abundance has increased while oxygen stays the same. The thick purple line shows the chemistry for TiO, which shows a considerable decrease in abundance when the C/O ratio is higher.

seen in the simulated chemistry shown in Figure 3.2, as a large decrease in TiO abundance is seen when the C/O ratio is > 1.0.

In Figures 3.3-3.4, we see the chemistry of Ti-bearing and V-bearing species for the temperatures 2000 K and 3000 K, modelled with `FastChem`. In the former, we have solar metallicity, and in the latter, we have a metallicity 20 times higher. For 2000 K at solar metallicity, we see that Ti, V, TiO, and VO are most abundant. However, as expected, Ti II and V II become more abundant in the upper parts of the atmosphere at 3000 K.

We also note that for 2000 K, there is a bump at roughly 10^{-6} bar for Ti and V, which correlates to the turn-off point for TiO_2 and VO_2. Although not as prominent, this feature can still be seen for Ti at 3000 K. When we increase the metallicity to 20 times greater than solar, we see this bump for TiO and VO, and these two species are of great interest. The other species show this turn-off or bump too.

Astrophysicists have proposed that there should be TiO and VO in some of these hot objects. One of the reasons to look for TiO and VO is that we have seen them commonly in brown dwarfs. Arguably, gas giants and brown dwarfs share similar characteristics, such as fundamental dynamical, physical, and chemical processes. These characteristics shape the circulation and structure of atmospheres Showman et al. (2020). TiO and VO in gaseous form strongly absorb UV and visible light. This would heat the upper atmosphere, as suggested by Fortney et al. (2008), leading to a rise in temperature with altitude and thus resulting in a thermal inversion. So astronomers have been extensively searching for any sign of TiO and VO for a decade. However, Spiegel et al. (2009) found in their study of irradiated giant planets that VO is unlikely to play a role in the thermal inversion, and macroscopic mixing is essential for the TiO thermal inversion hypothesis to hold.

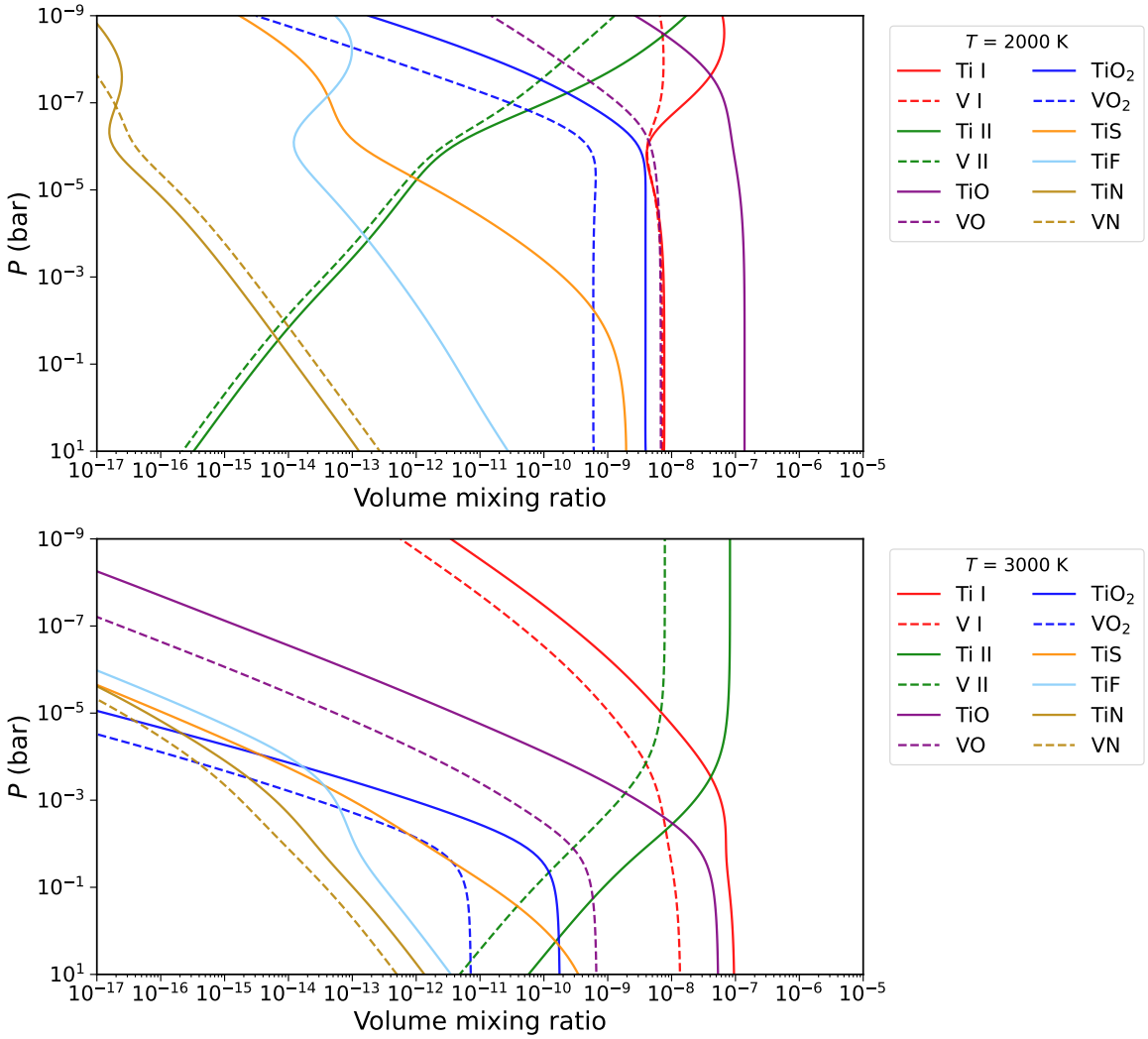

Figure 3.3: The two figures show the chemistry of Ti-bearing and V-bearing species at solar metallicity for 2000 K (top) and 3000 K (bottom), both modelled with `FastChem`. On the x-axis we have the volume mixing ratio, and on the y-axis we have the pressure.

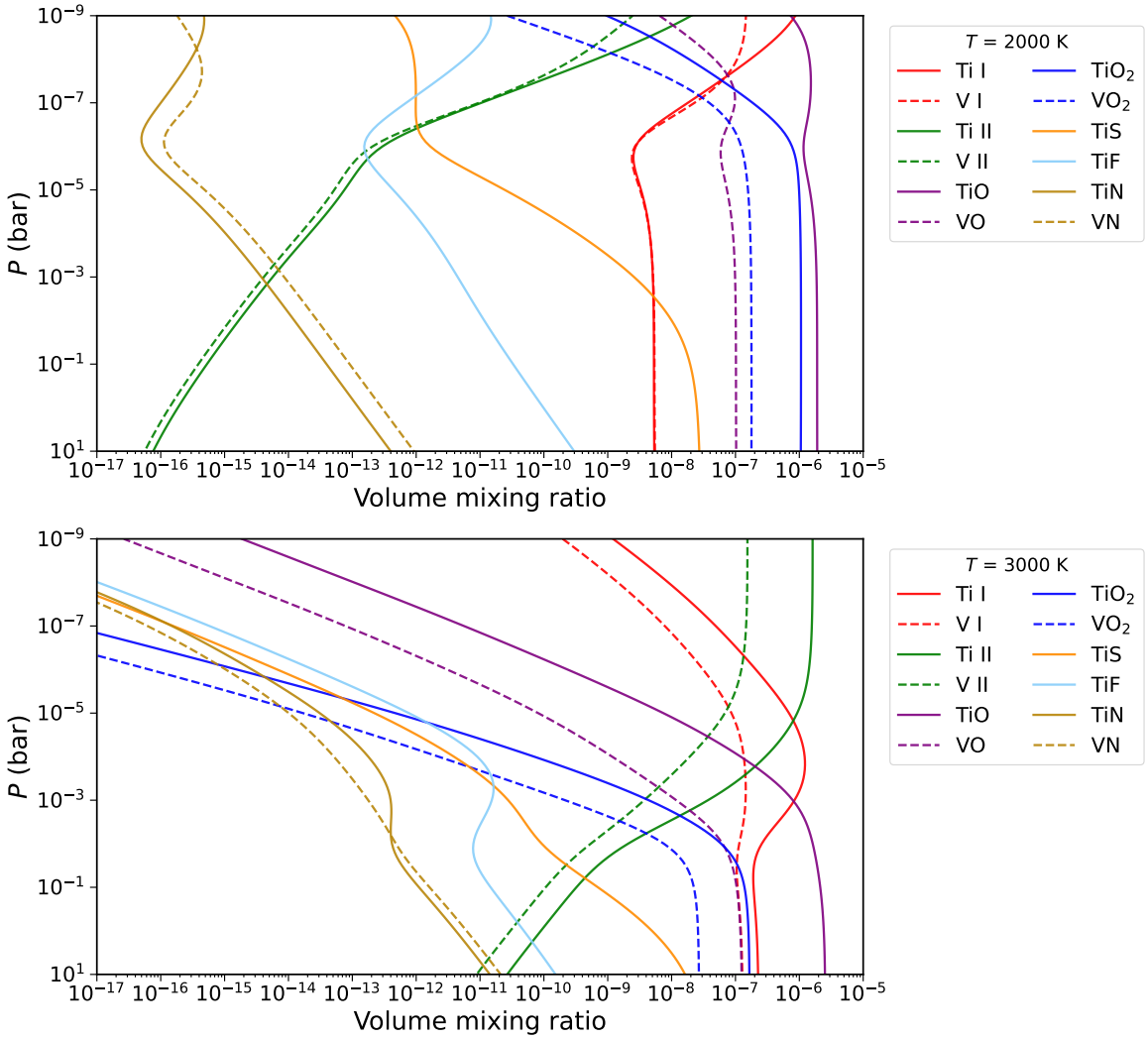

Figure 3.4: The figures show the same as Figure 3.3, though for a metallicity 20 times greater than solar.

3.3 Linking the codes

Firstly, the output from `FastChem` labels the species' names in alphabetical order, i.e. TiO would be O1Ti1, CO would be C1O1, and some would include an underscore and the order of configuration. For example, they denote CN_2 as either C1N2_cnn or C1N2_ncn, depending on the isomer. Isomers have the same chemical formula but differ in their configuration. These names had to be changed so the code could read and convert them into mass fractions instead.

As mentioned in section 3.1, `petitRADTRANS` needs the mass fractions of species to compute spectra. We wrote an algorithm using the `periodictable` package in Python to calculate the atomic weight of all the different species with their VMR computed by `FastChem`. We would first compute each species' atomic mass, e.g. by reading C1O2 as `C.mass + O.mass*2`. We then convert these into mass fractions through

$$X_i = \frac{\mu_i}{\mu} n_i, \tag{3.3}$$

where for species i: X_i is the mass fraction, μ_i is the mass of a single molecule, atom or ion, μ is the atmospheric mean molecular weight, and n_i is the VMR.

We can then use the two codes to produce spectra without initially knowing any abundances.

3.4 Error estimation

When comparing the solution by `petitRADTRANS` to the one by HK17, we need to estimate how well the transmission spectra they have produced correlate. We initially used the R^2-score, where the closer it is to 1, the better they correlate. It is defined as

$$R^2 = 1 - \frac{SS_{\text{res}}}{SS_{\text{tot}}}, \tag{3.4}$$

where SS_{res} is the residual sum of squares and SS_{tot} is the total sum of squares. If $SS_{\text{res}} = 0$ then the two models correlate perfectly and $R^2 = 1$. However, since many data points on the transmission spectrum are shallow lines or continuum, these influenced the error estimation to the point where it was not representative of how good the fit was. As a result, we computed scores that did not feel like they accurately described the correlation. So, instead, we decided to use the reduced χ^2-score to describe the correlation between models.

The χ^2 method is commonly used in statistics to compare models to data and see which model fits the data best (Andrae et al. 2010). The reduced χ^2 is defined as χ^2 per degree of freedom,

$$\chi^2_{\text{red}} = \frac{\chi^2}{K}, \tag{3.5}$$

where K denotes the number of degrees of freedom. $K = i - m$ where i is the number of observations and m is the number of fitted parameters. χ^2 itself is the weighted sum of squared deviations as

$$\chi^2 = \sum_{n=1}^{N} \frac{(O_n - C_n)^2}{\sigma_n^2}, \tag{3.6}$$

where σ_n^2 is the variance, O is the observations or data, and C is the calculated model.

We use the Python package `scipy.stats.chisquared` to calculate our χ^2_{red} values. The method treats the variance through Pearson's chi-squared statistic, which sets the variance equal to the calculated model, i.e. $\sigma_n^2 = C_n$ (Pearson 1900).

In our case, the data will be the solution by HK17, and the models will be the solution of `petitRADTRANS` by varying parameters. If $\chi^2_{\text{red}} \gg 1$, it means that we have a poor fit. If $\chi^2_{\text{red}} > 1$, then the model does not correlate to the data well, and if we have $\chi^2_{\text{red}} < 1$, it indicates that we have an "over-fit" of the data. In our case, however, a reduced χ^2 score of zero means we have identical transmission spectra, and the correlation is perfect.

Chapter 4

Results

4.1 Analytical approximation & `petitRADTRANS`

We wish to reproduce the results of HK17 at high spectral resolution and low spectral resolution. In Figure 4.1, we compare the transmission spectra modelled with `petitRADTRANS` and the analytical approximation by HK17 at high spectral resolution. We have used the same parameters for the model as HK17 and looked specifically at the water absorption features from 1.15 to 1.65 μm. In Figure 4.1, we have the modelled transmission spectrum in the top figure and the residuals are shown in the bottom. The residuals are simply the difference between the `petitRADTRANS` solution and the HK17 solution, for each spectral line.

The parameters needed for computation are seen in Table 4.1. We determine the water mass fraction through `FastChem`, but we choose a singular constant abundance to be the maximum abundance out of those computed, which is 3.73×10^{-3}. However, we will investigate other abundances in section 4.1.5. The MMW is chosen at its value where the atmospheric pressure is 1 bar, where it is equal to 2.33. This value is consistent with an H_2 dominated atmosphere, and it is a very common assumption for hot Jupiters.

Table 4.1: The parameters for HD 209458b by Heng & Kitzmann (2017), where T is the temperature, $R_\star$ is the host star's radius, R_p is the planetary radius, g_0 is the surface gravity, P_0 is the surface pressure, and MMW is the mean molecular weight.

Parameters from Heng & Kitzmann (2017)					
T [K]	$R_\star$ [$R_\odot$]	R_p [R_{jup}]	g_0 [cm/s^2]	P_0 [bar]	MMW
1500	1.148	1.25	1000	10	2.33

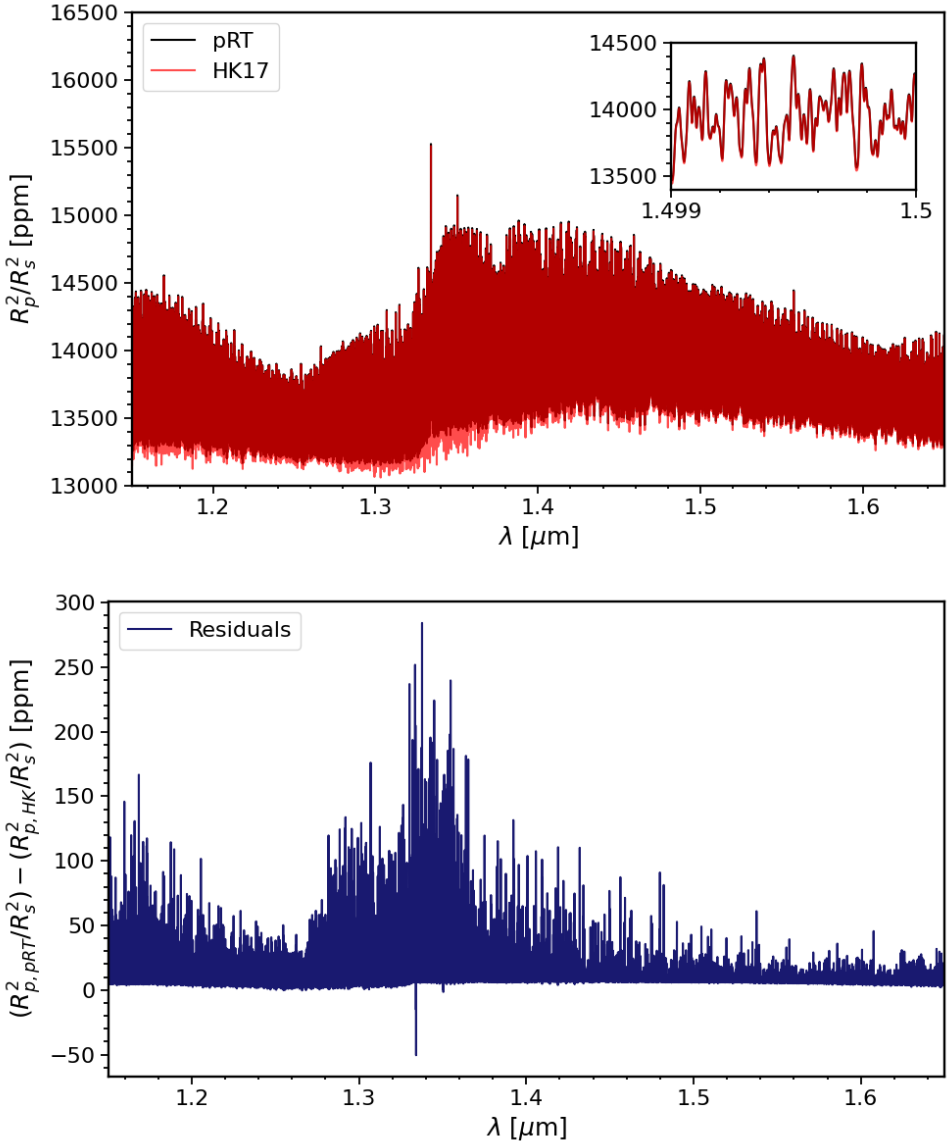

Figure 4.1: The upper figure shows the comparison between transmission spectra of H_2O computed by `petitRADTRANS` in black and the results from solving the analytical approximation by HK17 in red. The lower figure shows the residuals between the solutions for each spectral line.

We model the atmospheric pressure logarithmically spaced between 10 bar to 0.1 nbar, in 111 steps. We retrieve the opacity function used for the analytical approximation from `petitRADTRANS` at 1 mbar. It is worth noting that the `petitRADTRANS` solution uses multiple opacity functions for each iteration of the pressure, because the opacity is pressure dependent. It follows that due to the opacity function being dependent on pressure, we will end up with pressure broadening of our spectral lines. We only use the lines for species we

are investigating, which in this case is H_2O. This will remain the case for all the following results, where we only use the lines of the specific species we investigate. We also do not include the full chemical network of over 500 species computed by `FastChem`, we only include the species directly related. In reality, the spectrum would be crowded with lines from many species. For the sake of clarity, analysis, and comparison, we only include the one we investigate.

We see that even for high-resolution, the approximation correlates well with the solution of `petitRADTRANS`. Furthermore, in the zoomed-in window with 1 nm width, we see that the individual lines match each other well. Although there is a slight offset, the similarity between the two convinces HK17 of the accuracy of their model. We aim to explore whether this model is realistic since it does not include a number of physical effects, such as mass fractions that vary with pressure, or gravity that varies with altitude.

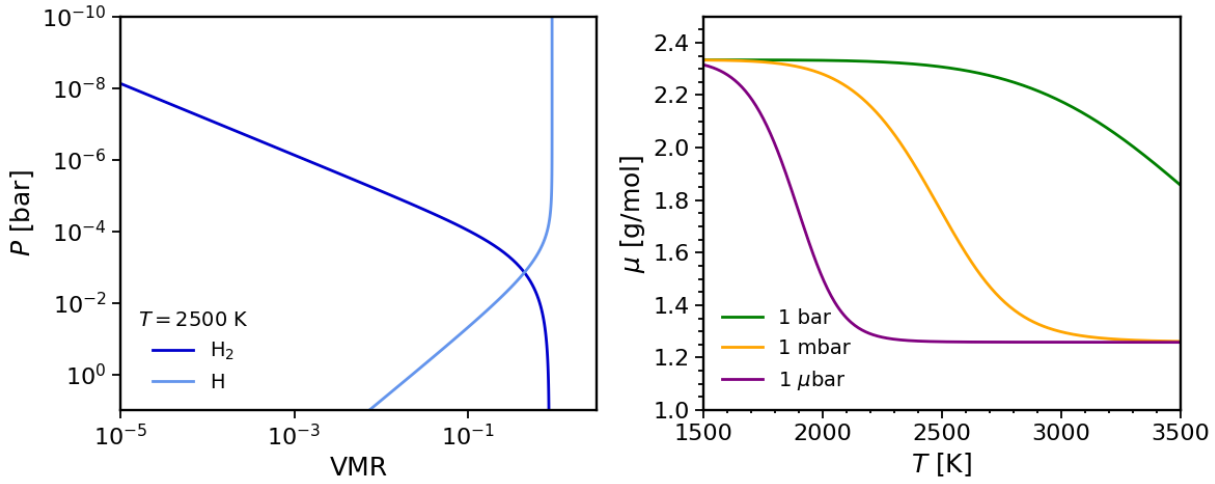

Figure 4.2: The left figure shows how the VMR of H_2 (dark blue) and H (light blue) change throughout a planetary atmosphere at 2500 K. In the upper atmosphere, H is most abundant due to the dissociation of H_2. The right figure shows how the MMW μ changes for different pressures in an atmosphere as we increase the temperature in steps of 5 K. The green line shows μ for 1 bar, the orange line for 1 mbar, and the purple line for 1 μbar.

4.1.1 Including variable mass fractions

We now include varying chemical abundances and MMW from `FastChem` depending on the pressure in the isothermal atmosphere. The MMW is dependent on the pressure and temperature, i.e. $\mu(P, T)$, due to the dissociation of H_2 into H. An example of this can be seen in the left plot of Figure 4.2. For a planet with a temperature of 2500 K, H is dominant in the upper atmosphere, where H_2 dissociates. Near the surface, where energetic photons are less likely to penetrate the atmosphere and dissociate H_2, we see that it is much more abundant than H. However, we are working with equilibrium chemistry where we neglect photochemistry. Instead, we have that H is favoured at low pressures and high temperatures, and H_2 is favoured at high pressures. To the right in Figure 4.2, we see how the MMW changes depending on the temperature and pressure.

The result of including mass fractions and MMW, which change with altitude, is seen in Figure 4.3, where we have the transmission spectrum and the residuals between the solutions. The HK17 solution now overestimates the line strengths instead. The solution by `petitRADTRANS` is semi-realistic now, as it includes variable mass fractions and variable MMW caused by chemistry. However, we still wish to see the effect of variable gravity, as that is the most realistic case while still operating with an isothermal atmosphere.

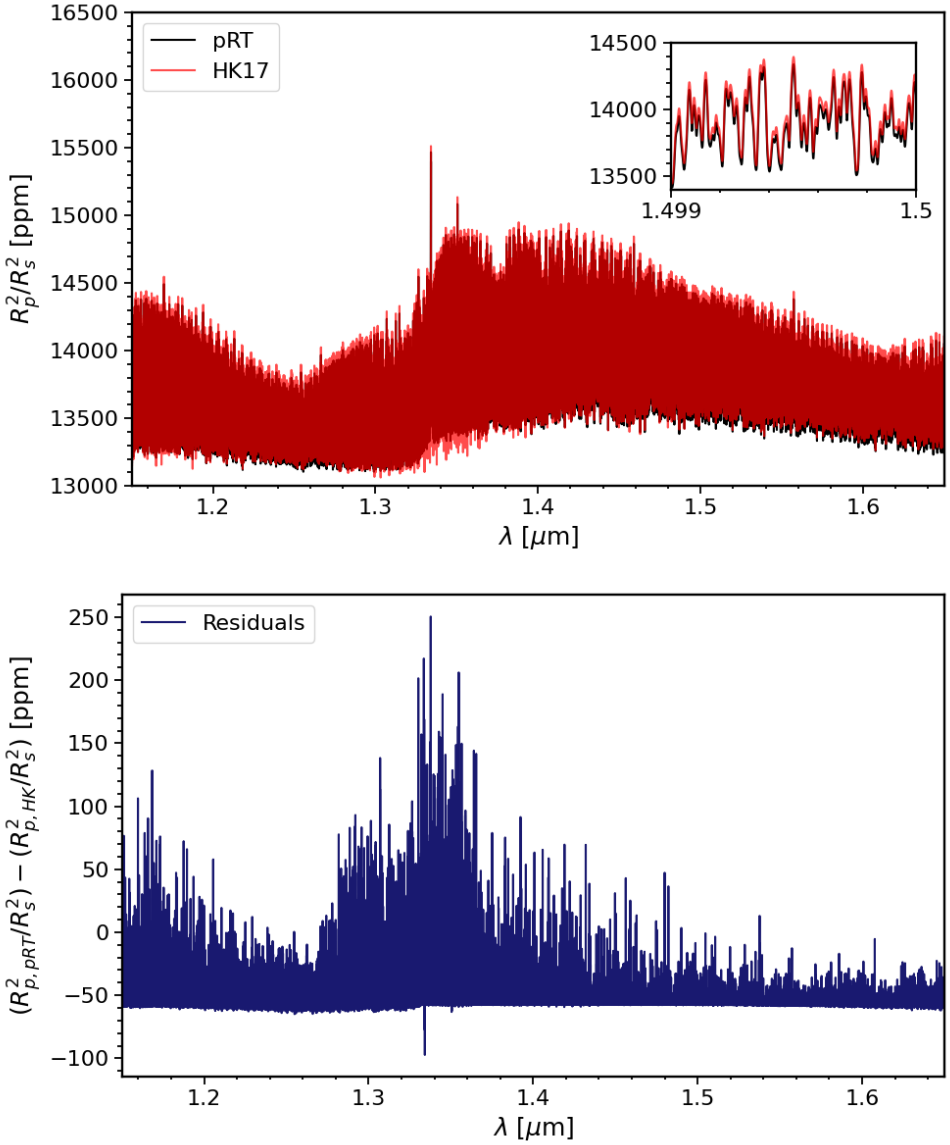

Figure 4.3: The upper figure shows the comparison between transmission spectra of H_2O computed by `petitRADTRANS` in black with variable abundance and the results from solving the analytical approximation by HK17 in red. The lower figure shows the residuals between the solutions for each spectral line.

4.1.2 Including variable mass fractions & variable gravity

We allow for pressure broadening in the petitRADTRANS solution by switching on variable gravity, which yields a larger scale height for the planetary atmosphere. The scale height is dependent on gravity and grows as the gravity decreases. Although the results of the two models (seen in Figure 4.4) are very similar, we see that the discrepancy between the two is larger than in Figures 4.1 and 4.3. This becomes especially clear when comparing the residuals in Figure 4.4 to the ones in Figures 4.1 and 4.3. So far, we have only investigated the models' correlations at a temperature of 1500 K, as was done in HK17. We need to investigate further to see if the models still correlate well and can be used for a broad range of temperatures.

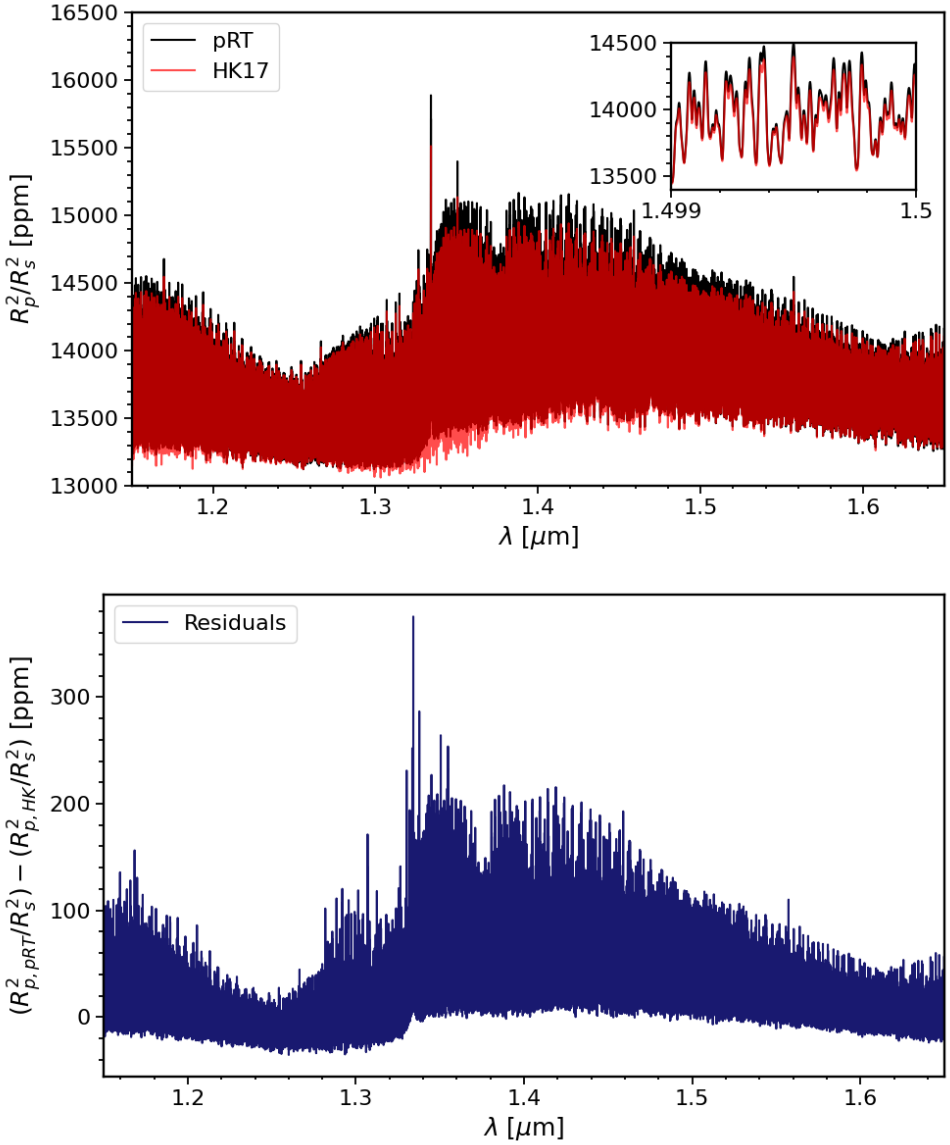

Figure 4.4: The upper figure shows the comparison between transmission spectra of H_2O computed by `petitRADTRANS` in black with variable abundance and variable gravity, and the results from solving the analytical approximation by HK17 in red. The lower figure shows the residuals between the solutions for each spectral line.

4.1.3 Comparing correlation for different temperatures

We will now visualise the correlation between the petitRADTRANS and HK17 solution for different temperatures. These figures include all three models from section 4.1 in the middle column and state their reduced χ^2 value. We abbreviate these models as:

- **Real:** Realistic version of petitRADTRANS, where we have a variable abundances and MMW ($X = X(r)$, $\mu = \mu(r)$) from FastChem, and variable gravity ($g = g(r)$).
- **Semi:** Semi-realistic version of petitRADTRANS, where we have a variable abundances and MMW ($X = X(r)$, $\mu = \mu(r)$) from FastChem, but a constant gravity ($g = g_0$).
- **Approx:** Approximate version of petitRADTRANS, where we have a constant abundance and MMW ($X = X_C$, $\mu = \mu_C$), as well as a constant gravity ($g = g_0$). This solution matches the conditions of HK17 best.

We will compute the transmission spectra for the three models and analytical approximation for three temperatures; 1500 K, 2500 K, and 3500 K. Since we now vary the temperature, keeping the MMW at 2.33 will no longer be accurate at higher temperatures due to the dissociation of H_2 which yields a smaller MMW at high temperatures. The MMW has a significant impact on the transmission spectrum, and we choose our MMW deep in the atmosphere at 1 bar, since the optical depth is large there and reflects on the bulk state of hydrogen.

At 1 bar pressure in the atmosphere, the MMW is calculated by FastChem to be 2.31 for 2500 K and 1.86 for 3500 K. The MMW at 1 bar follows the trend in green shown in Figure 4.2. We see the results of the computations in Figure 4.5. Although the approximate model uses a constant MMW, it still does comparatively well computing a transmission spectrum similar to the advanced models for 1500 K and 2500 K. When the temperature reaches 3500 K, that changes. We can no longer use the constant MMW and mass fraction as a good approximation for our spectra.

In the right column of Figure 4.5, we show the mass fractions of H_2O and H, and a dashed red line indicating the chosen constant abundance. We include H in the plot to illustrate how the MMW changes throughout the pressures in the atmosphere. When H is less abundant, we get a higher MMW and vice versa.

The mass fraction of H_2O vastly changes throughout the atmosphere at 3500 K, making it most abundant near the surface and rapidly decreasing as we approach low pressures. Therefore, we will also need to investigate the impact of abundance choice on the results. We explain this further in section 4.1.5.

Table 4.2: The reduced χ^2 scores between HK17's analytical approximation and petitRADTRANS models for H_2O at high resolution for 1500 K, 2500 K, and 3500 K.

Reduced χ^2 of H_2O for three temperatures			
T / Model	1500 K	2500 K	3500 K
Realistic	0.10	4.08	96.17
Semi-realistic	0.22	0.10	153.63
Approximate	0.01	0.02	0.15

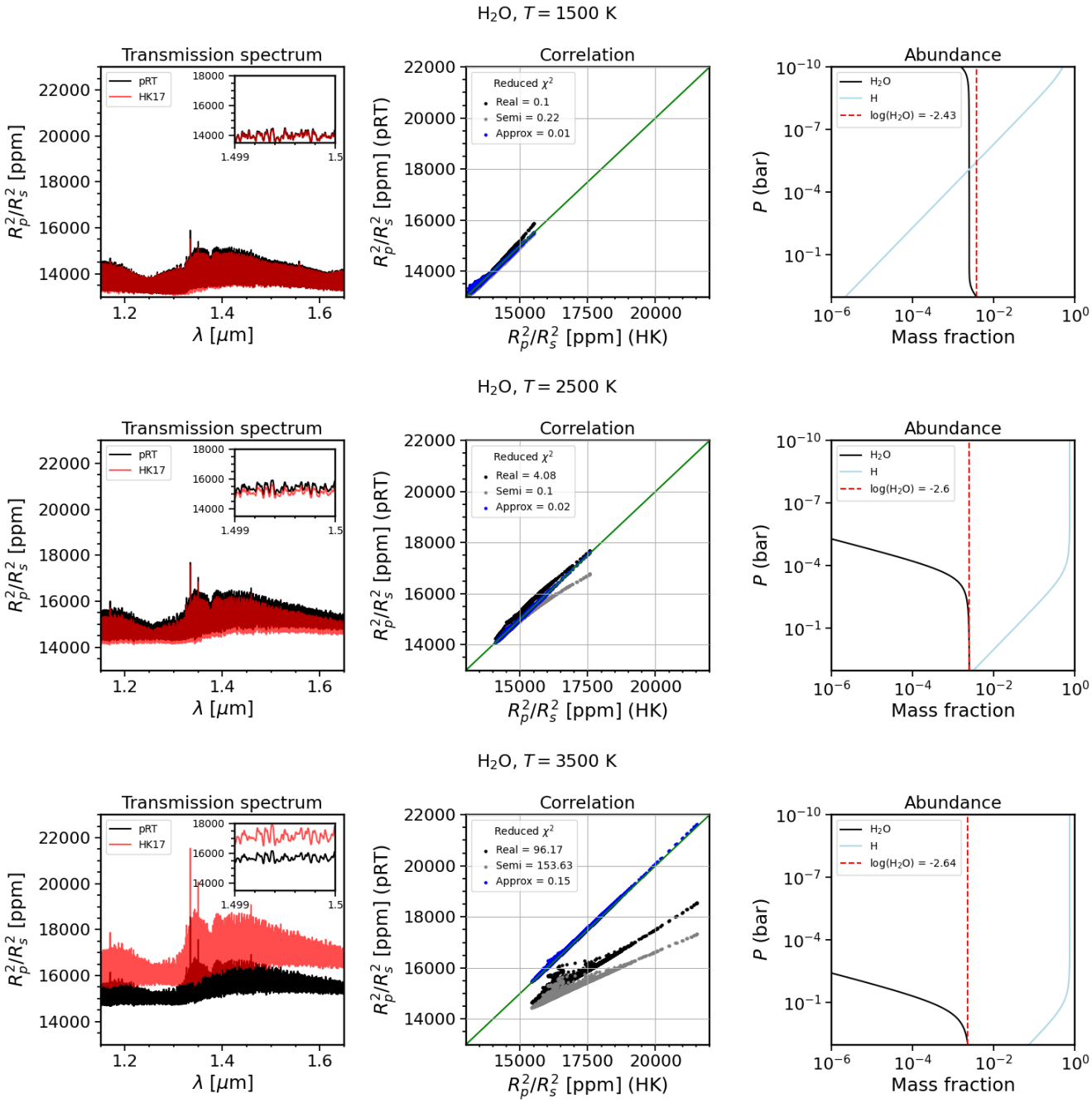

Figure 4.5: The left column shows the transmission spectrum produced by `petitRADTRANS` in black, where we have the realistic case. Red shows the solution by HK17's analytical approximation. The middle column shows the correlation between the different solutions of `petitRADTRANS` and HK17's analytical approximation. The realistic case is shown in black, the semi-realistic in grey, and the approximation in blue. We also display the reduced χ^2 value for each correlation. The right column shows the mass fractions of H_2O in black and H in light blue. The dashed red line indicates which mass fraction is used when we have a constant abundance. The rows represent temperatures of 1500 K, 2500 K, and 3500 K.

4.1.4 Low-resolution

Since HK17 use low-resolution transmission spectroscopy to test their model, we wish to do the same. To do so, we have similarly binned down our high-resolution spectrum to a lower resolution of $R = 130$, which corresponds to the spectral resolution of WFC3. Our choice is motivated by the fact that the analytical approximation was originally derived and tested for the WFC3 water band detection on the HST. As a result, we have gone from having 361016 points to 500 points, and we see the results in Figure 4.6 for temperatures of 1500 K, 2500 K, and 3500 K. The reduced χ^2 values are shown for each model and temperature in Table 4.3. The reduced χ^2 values did not change for the approximate model compared to the high-resolution model. For the other two models, we see slight changes.

Table 4.3: The reduced χ^2 scores between HK17's analytical approximation and `petitRADTRANS` models for H_2O for 1500 K, 2500 K, and 3500 K.

Reduced χ^2 of H_2O for three temperatures at low resolution			
T / Model	1500 K	2500 K	3500 K
Realistic	0.06	4.15	97.63
Semi-realistic	0.21	0.07	156.00
Approximate	0.01	0.02	0.15

The discrepancy between temperatures for H_2O is better seen in Figure 4.6 than in Figure 4.5, as the difference between the `petitRADTRANS` solution and HK17's analytical approximation becomes clear from a simpler trend.

For the exoplanet HD 209458b, HK17's analytical approximation does an excellent job at computing a transmission spectrum very similar to more advanced models for both high and low spectral resolution. However, this only holds for when the temperature is 1500 K, up to 2500 K. Due to variable gravity, larger scale height, variable mass fraction and MMW, the approximation breaks at higher temperatures and can no longer compete with advanced numerical methods. However, its application for hot Jupiters is remarkable for the water band. We have not detected many hot Jupiters with a temperature as high as 3500 K. One must, however, be careful when using the analytical approximation and make sure that applying it to their data is logical and within the scope of HK17's solution.

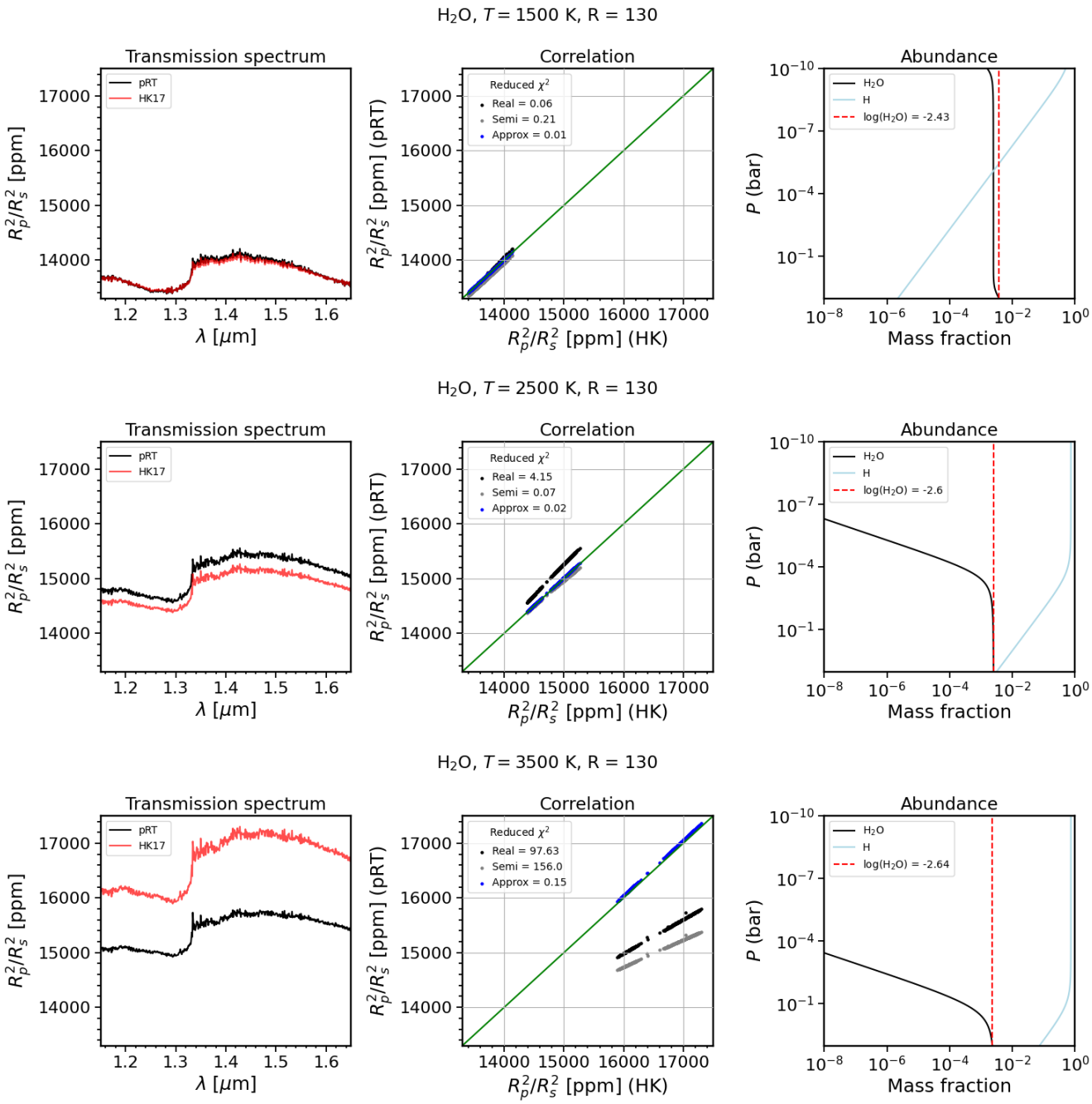

Figure 4.6: The left column shows the low-resolution transmission spectrum. In black, we have `petitRADTRANS`' realistic case. Red shows the solution by HK17's analytical approximation. The middle column shows the correlation between the different solutions of `petitRADTRANS` and HK17's analytical approximation. The realistic case is shown in black, the semi-realistic in grey, and the approximation in blue. We also display the reduced χ^2 value for each correlation. The right column shows the mass fractions of H_2O in black and H in light blue. The dashed red line indicates which mass fraction is used for a constant abundance. The rows represent temperatures of 1500 K, 2500 K, and 3500 K.

4.1.5 Varying the constant abundance

We will now investigate what happens if we vary the constant abundance used for HK17 and the approximate model. Since the realistic and semi-realistic models already include variable mass fractions, these remain the same throughout the process. We compute models for a temperature of 3500 K, since the H_2O abundance varies drastically throughout an atmosphere with such a temperature. We investigate the three mass fractions $\log(X_{H_2O}) = -2.6, -5.3, -8.0$, and their reduced χ^2 scores are stated in Table 4.4. We see that our choice of constant abundance significantly affects the results. Even though the mass fraction of H_2O varies greatly throughout the atmosphere, the best fit for a model with constant abundance would be one near the surface at higher pressures.

Table 4.4: The reduced χ^2 scores between HK17's analytical approximation and `petitRADTRANS` models for H_2O for a temperature of 3500 K with three different constant mass fractions for H_2O; $\log(X_{H_2O}) = -2.6, -5.3, -8.0$.

Reduced χ^2 of H_2O for three constant mass fractions			
$\log(X_{H_2O})$ / Model	-2.6	-5.3	-8.0
Realistic	111.78	25.92	117.02
Semi-realistic	0.91	8.88	26.38
Approximate	0.91	2.28	5.99

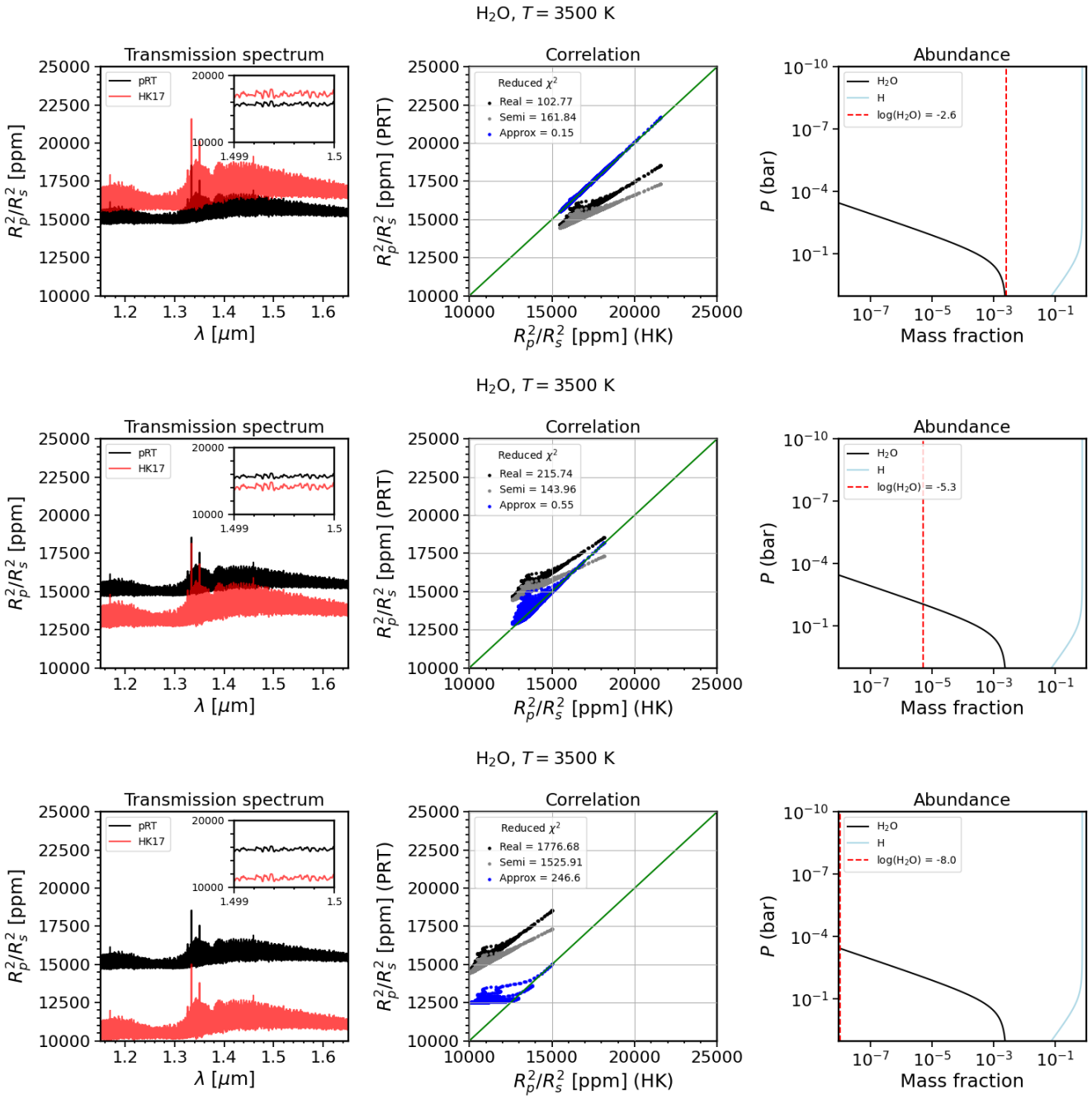

Figure 4.7: The left column shows the high-resolution transmission spectrum. In black, we have `petitRADTRANS`' realistic case. Red shows the solution by HK17's analytical approximation. The middle column shows the correlation between the different solutions of `petitRADTRANS` and HK17's analytical approximation. The realistic case is shown in black, the semi-realistic in grey, and the approximation in blue. We also display the reduced χ^2 value for each correlation. The right column shows the mass fractions of H_2O in black and H in light blue. The dashed red line indicates which mass fraction is used for a constant abundance. The rows represent constant abundances of $\log(X_{H_2O}) = -2.6, -5.3, -8.0$.

4.2 CO & Fe

Now that we have investigated where the analytical approximation holds for H_2O, we wish to investigate other species. The HK17 approximation was derived for the WFC3 water band, but others have used it to determine the abundances of other species, such as Fe, Ti, V, Mg, and Cr (Gibson et al. 2022). We wish to investigate if the analytical approximation may yield accurate abundance retrievals for these species or if it falls short, and how this may depend on the parameters of the exoplanet.

Due to their different molecular and atomic properties, CO and Fe are two attractive targets to analyse. Fe has the highest binding energy of all atoms and has strong spectral lines between 0.3-0.7 μm, including some of the UV and visible electromagnetic spectrum. One of the most important aspects of studying Fe in hot Jupiters is that Fe could be a major absorber in the stratosphere, leading to temperature inversions (Gibson et al. 2020). It has been observed in several ultra-hot Jupiters (Yan, F. et al. 2020), and the absorption of Fe lines at optical and UV wavelength regimes could produce temperature inversions without the presence TiO or VO (Lothringer & Barman 2019).

CO is an important molecule in astrophysics. It is one of the most strongly bound molecules and relatively abundant in the atmospheres of hot Jupiters. It has strong infrared absorption bands and can be used to constrain the C/O ratios of these planets (Madhusudhan 2012). Furthermore, due to its electronic structure being a light molecule, it is susceptible to theoretical analysis (Krupenie 1966).

For these species and others to follow, we have included clouds, because these spectra have fewer lines with significant gaps in between, by introducing κ_0 and γ into the model. They are related to the wavelength and opacity through

$$\kappa = \kappa_0 \left(\frac{\lambda}{\lambda_0} \right)^{\gamma}, \tag{4.1}$$

where $\lambda_0 = 0.35$ μm. We have set $\kappa_0 = 0.005$ cm^2/g, and for a flat opacity, we have that $\gamma = 0$ since γ sets the wavelength dependence. We include clouds to ensure that the continuum is flat. Since we have the flat continuum, unlike the water band investigated in section 4.1, we now subtract the continuum to illustrate the transit depth better. Furthermore, for the following sections, we extend our atmosphere to pressures up to 1 pbar and have 131 logarithmically spaced layers of pressure.

In Figure 4.8, we show the results of all three models compared to HK17's analytical approximation for the temperatures 1500 K, 2500 K, and 3500 K. The reduced χ^2 values for each temperature can be seen both in Figure 4.8 and in Table 4.5. Initially striking is that the correlation for all three models at 1500 K is decent, similar to the results for the water band in Figure 4.5. One might think that this is due to a nearly constant abundance of CO throughout the atmosphere, which is seen in the right column. However, as we increase the temperature to 2500 K and maintain an almost constant CO abundance, both the realistic and semi-realistic models diverge, and HK17 underestimates the line strengths. By the time we reach 3500 K, the transit radius computed by `petitRADTRANS` in the realistic model is nearly three times greater than HK17's approximation.

In Figure 4.9, we display the results in the same format as Figure 4.8, but for Fe instead. The reduced χ^2 scores can be seen in the middle column of Figure 4.9 and Table 4.6 for the three temperatures. It is clear that even though the correlation is not very good for lower temperatures, although still decent, it becomes much worse for high temperatures. The HK17 solution once again underestimates the line strengths when we include a varying mass fraction and variable gravity. As for CO, at 3500 K specific lines are roughly three times stronger when computed by the realistic `petitRADTRANS` model.

Table 4.5: The reduced χ^2 scores between HK17's analytical approximation and `petitRADTRANS` models for CO, for 1500 K, 2500 K, and 3500 K.

Reduced χ^2 of CO for three temperatures			
Model \ T	1500 K	2500 K	3500 K
Realistic	3.19	63.82	398.20
Semi-realistic	2.42	20.29	101.85
Approximate	2.42	7.78	24.62

Table 4.6: The reduced χ^2 scores between HK17's analytical approximation and `petitRADTRANS` models for Fe, for 1500 K, 2500 K, and 3500 K.

Reduced χ^2 of Fe for three temperatures			
Model \ T	1500 K	2500 K	3500 K
Realistic	3.89	111.54	641.65
Semi-realistic	2.69	24.03	84.28
Approximate	2.68	5.19	12.00

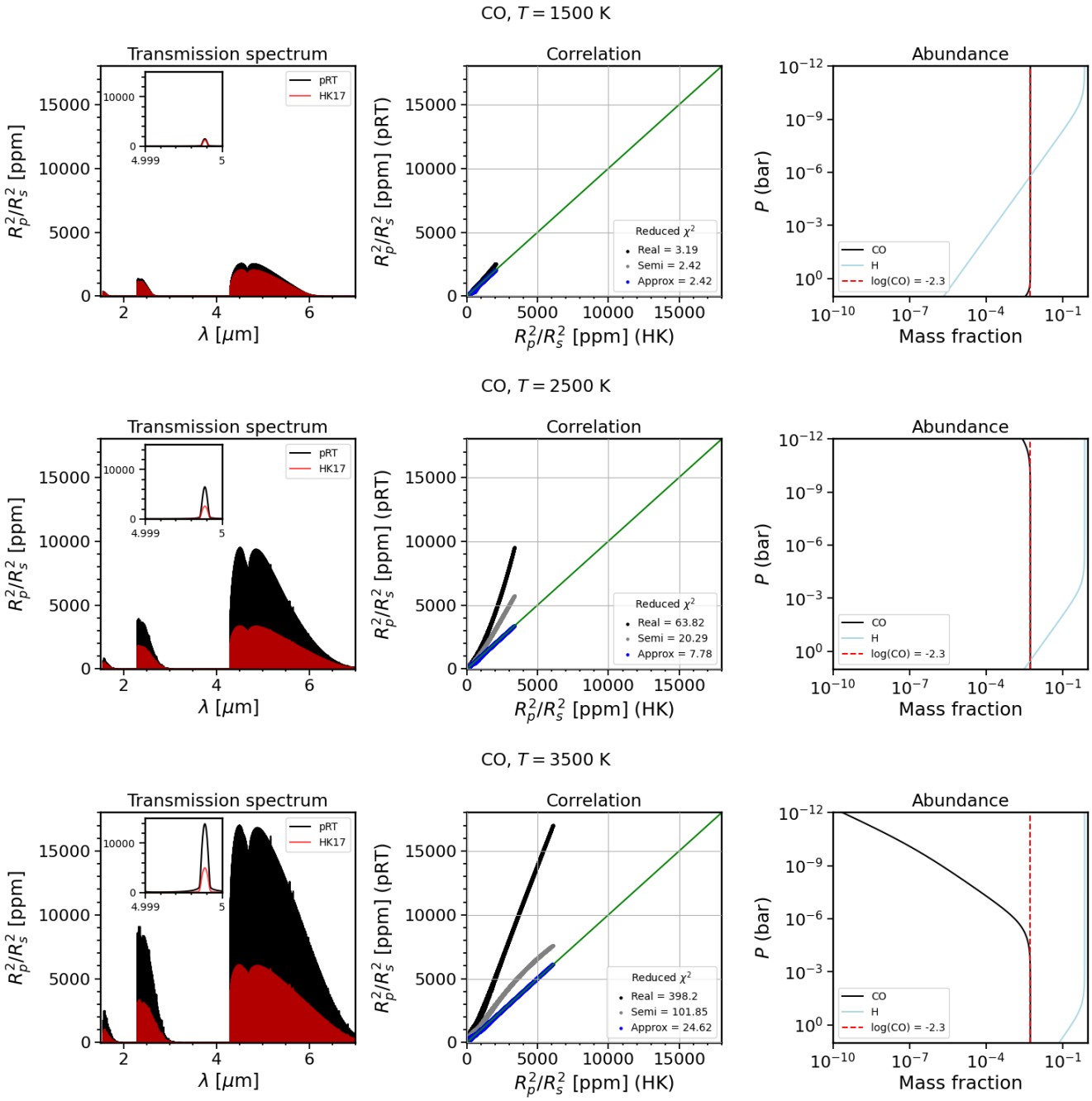

Figure 4.8: The left column shows the high-resolution transmission spectrum of CO. In black we have `petitRADTRANS`'s realistic case. Red shows the solution by HK17's analytical approximation. The middle column shows the correlation between the different solutions of `petitRADTRANS` and HK17's analytical approximation. The realistic case is shown in black, the semi-realistic in grey, and the approximation in blue. We also display the reduced χ^2 value for each correlation. The right column shows the mass fractions of CO in black and H in light blue. The dashed red line indicates which mass fraction is used for a constant abundance. The rows represent temperatures of 1500 K, 2500 K, and 3500 K.

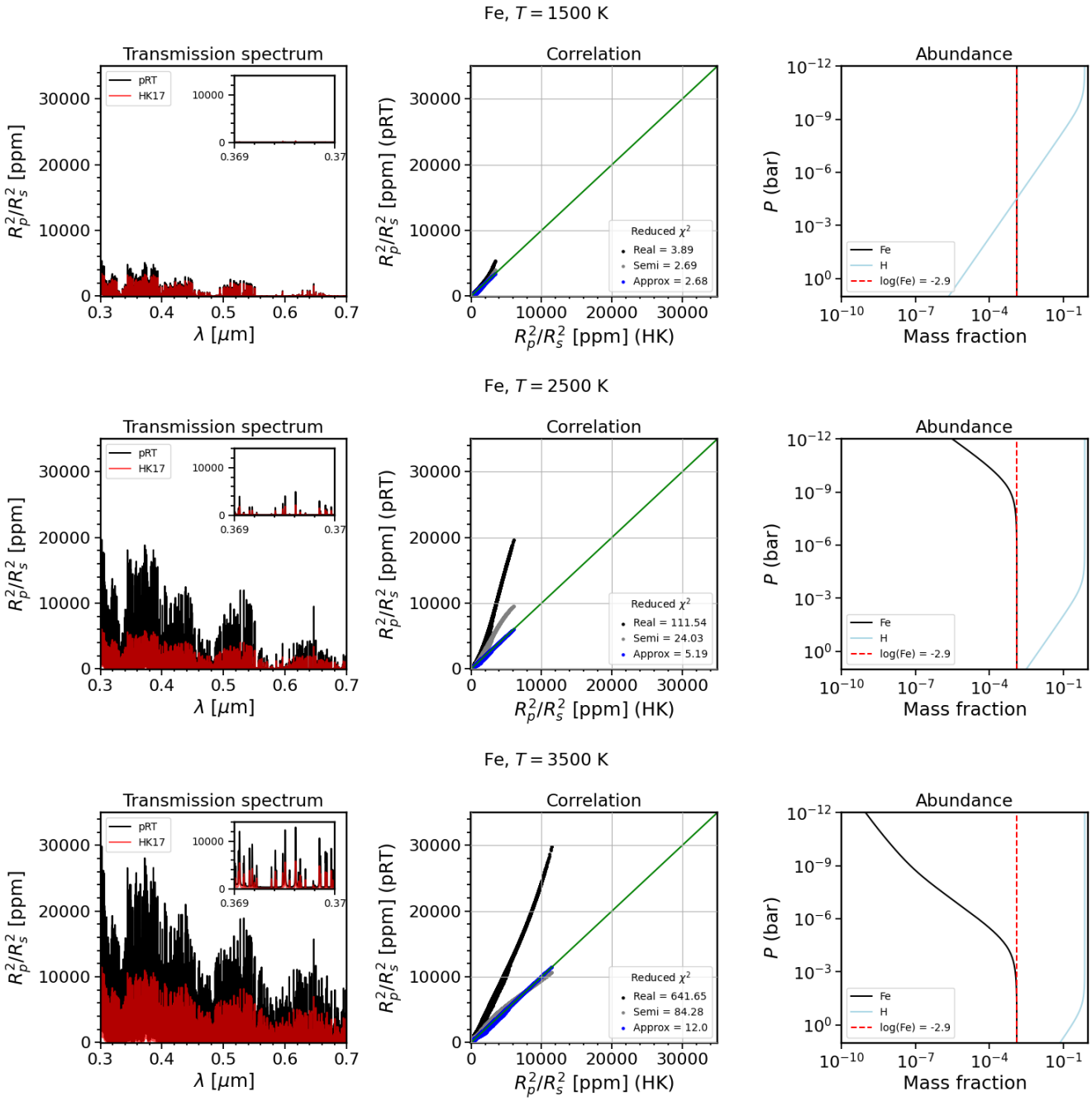

Figure 4.9: The left column shows the high-resolution transmission spectrum of Fe. In black we have `petitRADTRANS`'s realistic case. Red shows the solution by HK17's analytical approximation. The middle column shows the correlation between the different solutions of `petitRADTRANS` and HK17's analytical approximation. The realistic case is shown in black, the semi-realistic in grey, and the approximation in blue. We also display the reduced χ^2 value for each correlation. The right column shows the mass fractions of Fe in black and H in light blue. The dashed red line indicates which mass fraction is used for a constant abundance. The rows represent temperatures of 1500 K, 2500 K, and 3500 K.

4.3 Fe II

Fe II forms in the upper atmospheres of the hottest planets, with strong near-UV absorption lines, it can heat the upper atmosphere and cause thermal inversion, although this occurs at a much higher altitude than Fe (Gibson et al. 2020). For Fe II, we only show the 2500 K and 3500 K results since the spectral lines at 1500 K are virtually non-existent. Fe II is more prominent in hotter atmospheres and at lower pressures than close to the surface.

The results are seen in Figure 4.10 for the wavelength range of 0.3-0.55 μm, where for 2500 K, the HK17 solution greatly overestimates the line strengths. This is mainly due to the mass fraction of Fe II spanning many orders of magnitude but needs to be kept constant for the approximate model and HK17 solution. The realistic and semi-realistic `petitRADTRANS` solutions find that the spectral lines barely exist at 2500 K. When we increase the temperature to 3500 K, the HK17 solution instead underestimates the line strengths. Due to the effect of variable gravity, the correlation between the HK17 approximation and the realistic model of `petitRADTRANS` becomes poor. The reduced χ^2 scores can be seen in Table 4.7.

For Fe II, it becomes evident that the inclusion of variable mass fractions is crucial for species whose mass fraction spans many orders of magnitude throughout the atmosphere. Therefore, it is not advisable to use the HK17 approximation for abundance retrievals of Fe II. Furthermore, for species i where X_i increases with altitude, HK17 cannot be used simply because a representative value of the mass fraction cannot be found. Additionally, the effect of variable gravity is strongest in the upper atmosphere as the gravity decreases.

Table 4.7: The reduced χ^2 scores between HK17's analytical approximation and `petitRADTRANS` models for Fe II, for 2500 K and 3500 K.

Reduced χ^2 of Fe II for two temperatures		
Model \ T	2500 K	3500 K
Realistic	2.28	21.28
Semi-realistic	2.30	4.24
Approximate	0.04	0.11

Gibson et al. (2020) used an isothermal and isobaric atmosphere, where they detected Fe in the atmosphere of WASP121-b. As we see in Figure 4.9, their abundance retrievals are possibly underestimated since `petitRADTRANS` predicts much stronger spectral lines. They could not confirm any detection of Fe II in their analysis, and as we see in Figure 4.10, Fe II is very sensitive to both the varying abundance in the atmosphere and variable gravity. It is usually found in the upper layer of the atmosphere, where variable gravity needs to be accounted for to simulate an accurate scale height. The spectral lines for Fe II grow significantly between 2500 K and 3500 K, which means that the planet's temperature must carefully be considered to retrieve an accurate transmission spectrum for Fe II.

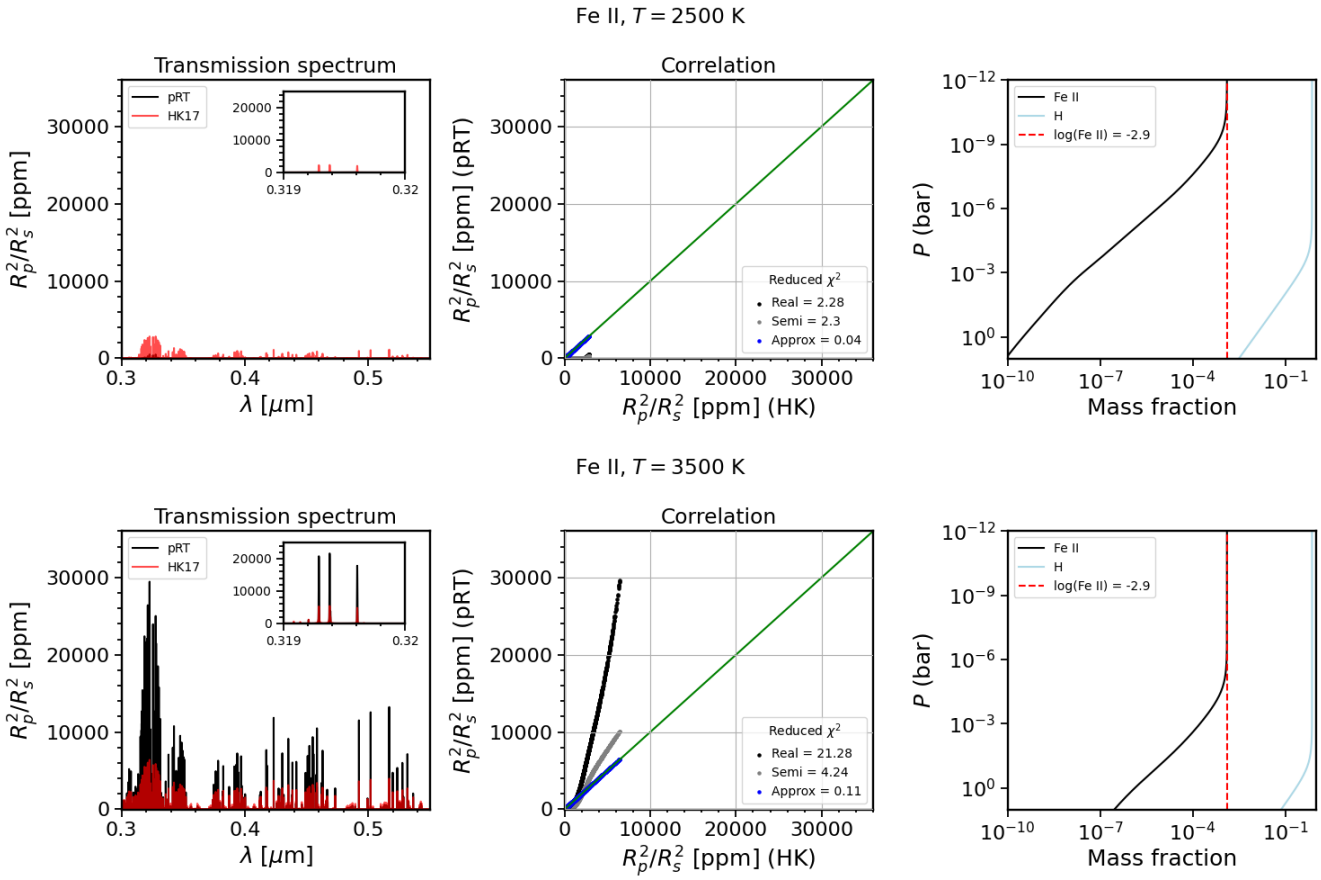

Figure 4.10: The left column shows the high-resolution transmission spectrum of Fe II. In black, we have `petitRADTRANS`' realistic case. Red shows the solution by HK17's analytical approximation. The middle column shows the correlation between the different solutions of `petitRADTRANS` and HK17's analytical approximation. The realistic case is shown in black, the semi-realistic in grey, and the approximation in blue. We also display the reduced χ^2 value for each correlation. The right column shows the mass fractions of Fe II in black and H in light blue. The dashed red line indicates which mass fraction is used for a constant abundance. The rows represent temperatures of 2500 K and 3500 K.

4.4 Ti, V, Mg, & Cr

In section 4.2, we mentioned that Gibson et al. (2022) had used an extended version of the HK17 approximation to determine the abundances of other species such as Ti, V, Mg, and Cr. Their analysis was made for WASP-121b, which is an ultra-hot Jupiter with an equilibrium temperature of over 2400 K. We will investigate these species at 1500 K, 2500 K, and 3500 K to see whether abundance retrievals without variable mass fractions, variable MMW, and variable gravity are accurate. However, we will compute the models with the parameters from HK17 shown in Table 4.1 to allow for comparison with the previous studies of H_2O, CO, Fe, and Fe II.

The models and reduced χ^2 scores for Ti are seen in Figure 4.11 and Table 4.8 for the wavelength range of 0.3-3.0 μm, and for V, they are seen in Figure 4.12 and Table 4.9 for the wavelength range of 0.3-2.3 μm. The results from the Mg-computations are seen in Figure 4.13 and Table 4.10 for the wavelength range of 0.3-0.6 μm, and for Cr in Figure 4.14 and Table 4.14 for the wavelength range of 0.3-1.5 μm. By simply looking at the reduced χ^2 scores, what initially catches the eye is that correlations for these species are much better than for CO, Fe, and Fe II.

Table 4.8: The reduced χ^2 scores between HK17's analytical approximation and `petitRADTRANS` models for Ti, for 1500 K, 2500 K, and 3500 K.

Reduced χ^2 of Ti for three temperatures			
Model \ T	1500 K	2500 K	3500 K
Realistic	0.52	6.55	5.52
Semi-realistic	0.57	1.51	5.22
Approximate	0.08	0.96	3.25

Table 4.9: The reduced χ^2 scores between HK17's analytical approximation and `petitRADTRANS` models for V, for 1500 K, 2500 K, and 3500 K.

Reduced χ^2 of V for three temperatures			
Model \ T	1500 K	2500 K	3500 K
Realistic	0.80	5.45	2.83
Semi-realistic	0.89	1.23	2.00
Approximate	0.11	0.34	0.92

Table 4.10: The reduced χ^2 scores between HK17's analytical approximation and `petitRADTRANS` models for Mg, for 1500 K, 2500 K, and 3500 K.

Reduced χ^2 of Mg for three temperatures			
Model \ T	1500 K	2500 K	3500 K
Realistic	0.66	7.52	49.04
Semi-realistic	0.23	2.06	9.84
Approximate	0.22	0.46	1.66

Table 4.11: The reduced χ^2 scores between HK17's analytical approximation and `petitRADTRANS` models for Cr, for 1500 K, 2500 K, and 3500 K.

Reduced χ^2 of Cr for three temperatures			
Model \ T	1500 K	2500 K	3500 K
Realistic	1.02	10.06	23.28
Semi-realistic	0.84	4.55	12.63
Approximate	0.84	2.58	9.24

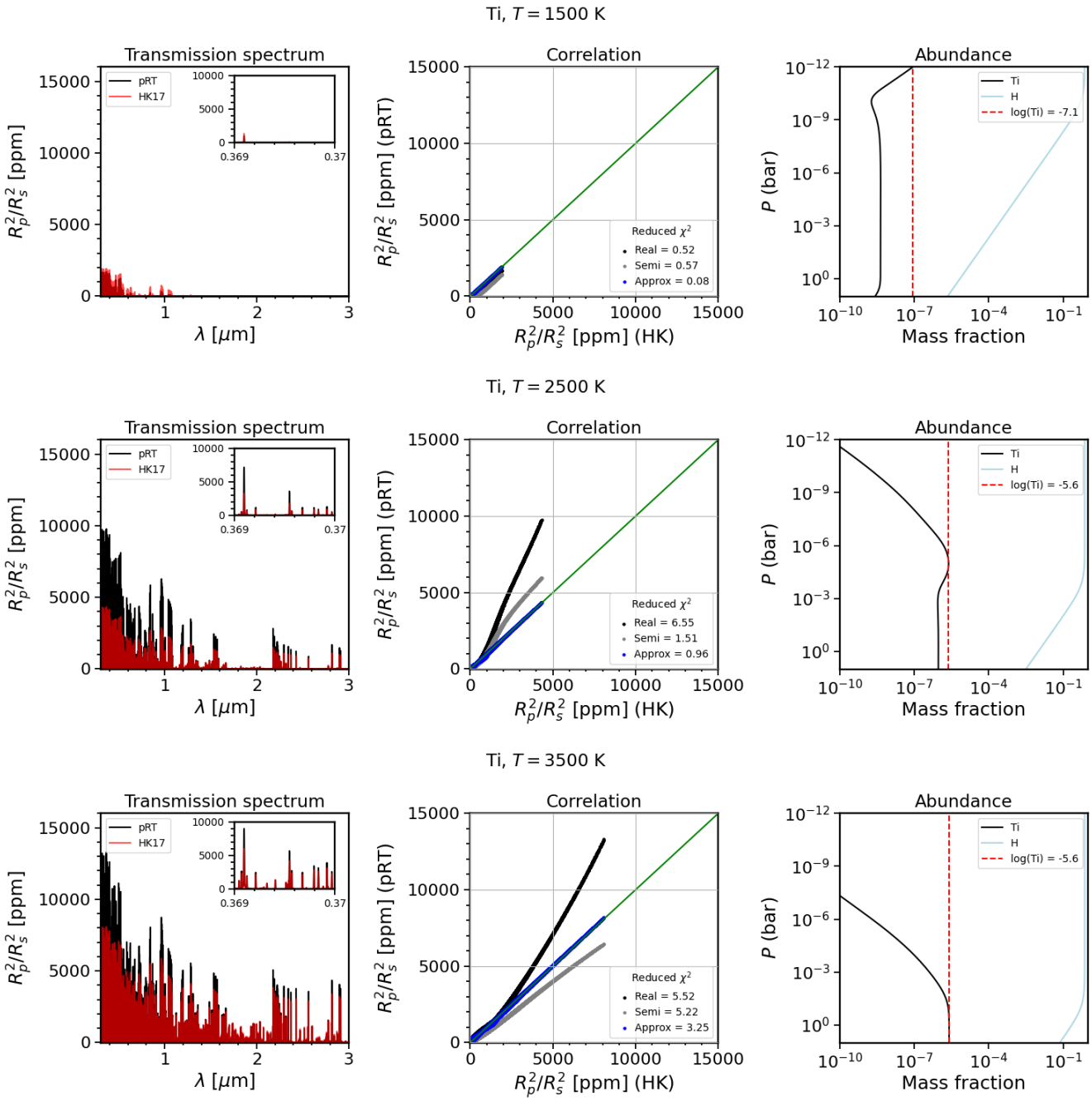

Figure 4.11: The left column shows the high-resolution transmission spectrum of Ti. In black, we have `petitRADTRANS`' realistic case. Red shows the solution by HK17's analytical approximation. The middle column shows the correlation between the different solutions of `petitRADTRANS` and HK17's analytical approximation. The realistic case is shown in black, the semi-realistic in grey, and the approximation in blue. We also display the reduced χ^2 value for each correlation. The right column shows the mass fractions of Ti in black and H in light blue. The dashed red line indicates which mass fraction is used for a constant abundance. The rows represent temperatures of 1500 K, 2500 K, and 3500 K.

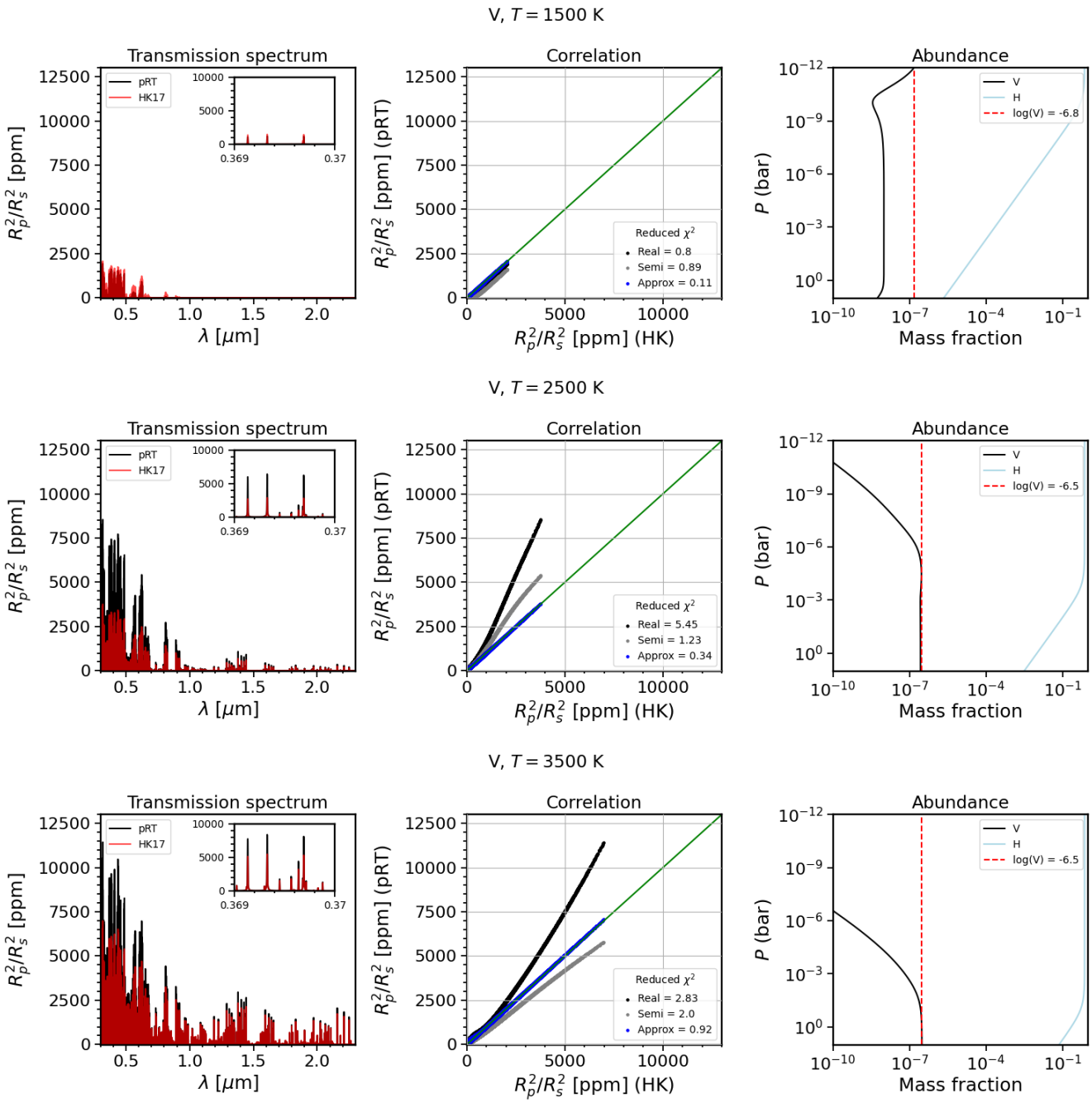

Figure 4.12: The left column shows the high-resolution transmission spectrum of V. In black, we have `petitRADTRANS`' realistic case. Red shows the solution by HK17's analytical approximation. The middle column shows the correlation between the different solutions of `petitRADTRANS` and HK17's analytical approximation. The realistic case is shown in black, the semi-realistic in grey, and the approximation in blue. We also display the reduced χ^2 value for each correlation. The right column shows the mass fractions of V in black and H in light blue. The dashed red line indicates which mass fraction is used for a constant abundance. The rows represent temperatures of 1500 K, 2500 K, and 3500 K.

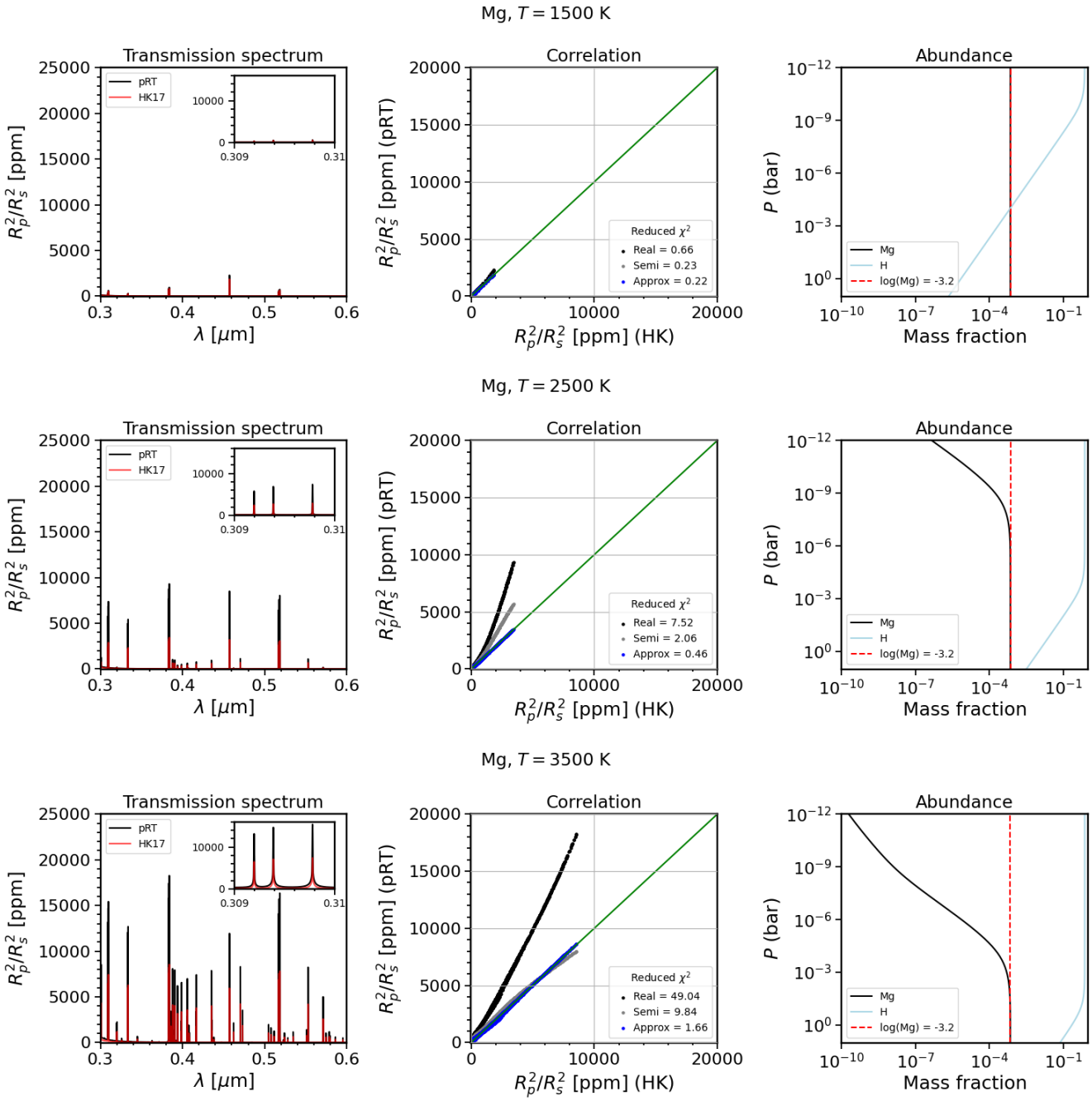

Figure 4.13: The left column shows the high-resolution transmission spectrum of Mg. In black, we have `petitRADTRANS`' realistic case. Red shows the solution by HK17's analytical approximation. The middle column shows the correlation between the different solutions of `petitRADTRANS` and HK17's analytical approximation. The realistic case is shown in black, the semi-realistic in grey, and the approximation in blue. We also display the reduced χ^2 value for each correlation. The right column shows the mass fractions of Mg in black and H in light blue. The dashed red line indicates which mass fraction is used for a constant abundance. The rows represent temperatures of 1500 K, 2500 K, and 3500 K.

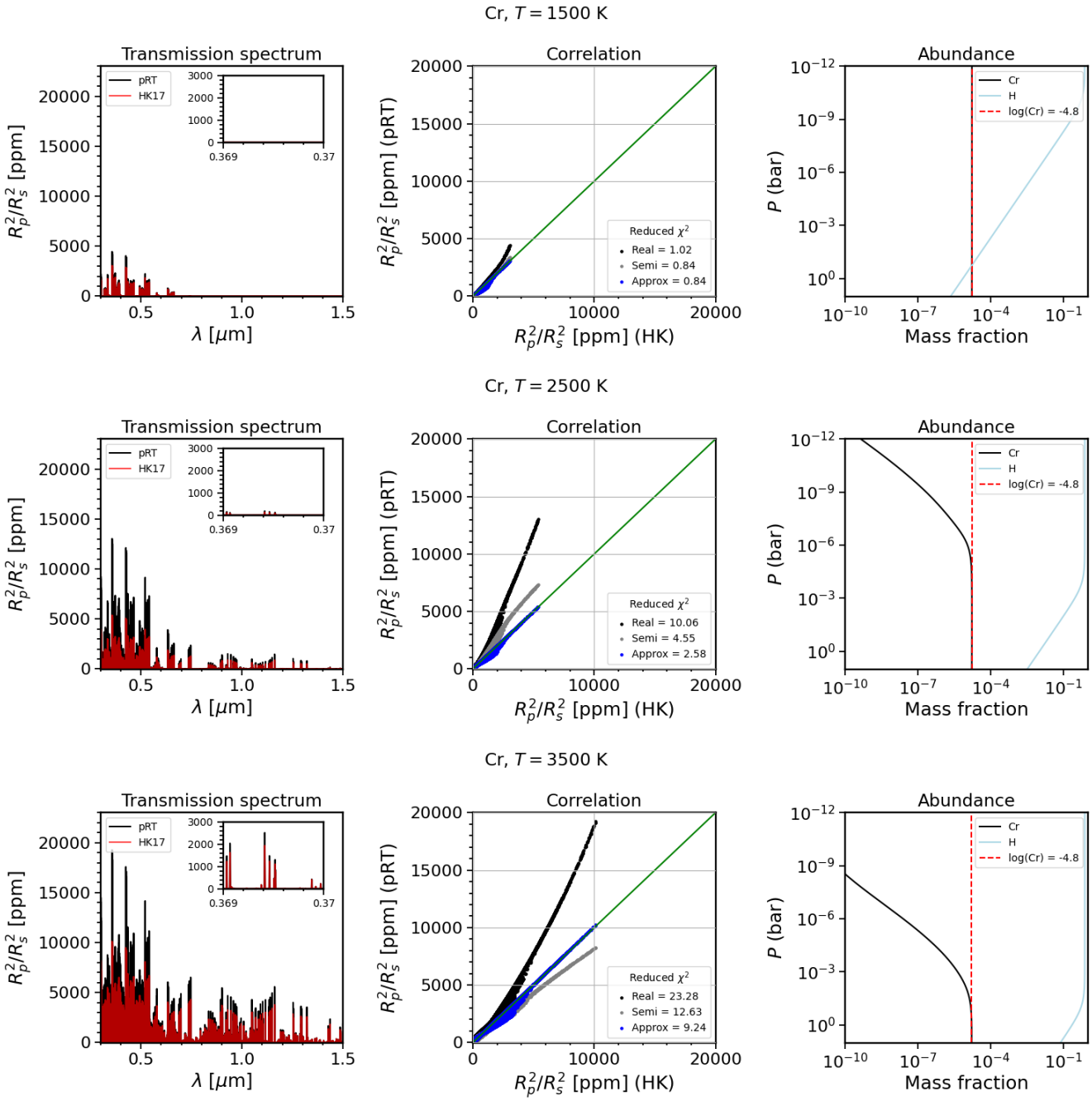

Figure 4.14: The left column shows the high-resolution transmission spectrum of Cr. In black, we have `petitRADTRANS`' realistic case. Red shows the solution by HK17's analytical approximation. The middle column shows the correlation between the different solutions of `petitRADTRANS` and HK17's analytical approximation. The realistic case is shown in black, the semi-realistic in grey, and the approximation in blue. We also display the reduced χ^2 value for each correlation. The right column shows the mass fractions of Cr in black and H in light blue. The dashed red line indicates which mass fraction is used for a constant abundance. The rows represent temperatures of 1500 K, 2500 K, and 3500 K.

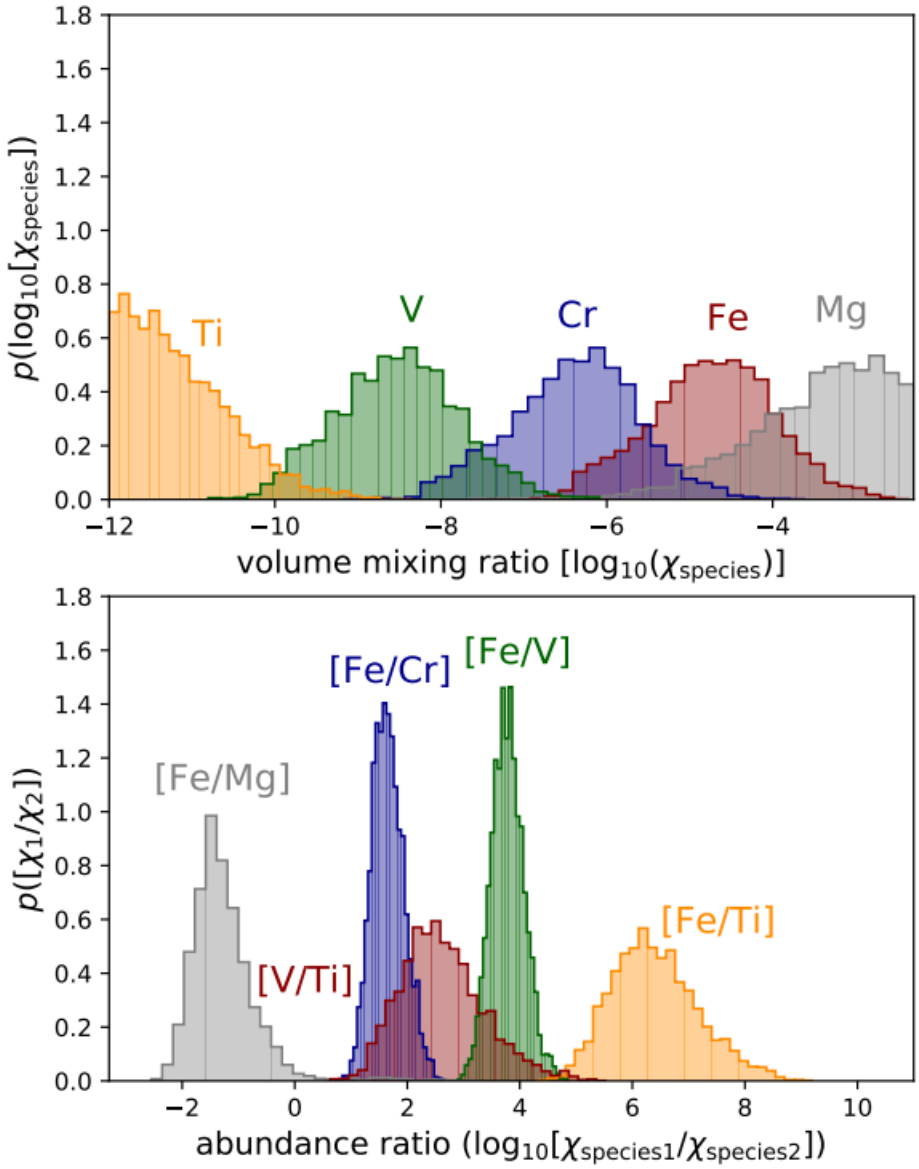

Figure 4.15: Abundances and relative abundances for WASP-121b adopted from Gibson et al. (2022), where they performed the retrieval on both UVES arms.

The analytical approximation computes decent transmission spectra for Ti, V, Cr, and Mg, at $T = 1500$ K. However, at 2500 K and 3500 K, the realistic and semi-realistic models begin to diverge. Since WASP-121b is an ultra-hot Jupiter with an equilibrium temperature over 2400 K, we cannot expect to use the HK17 approximation reliably.

We can conclude from the preceding results that HK17 does poorly differently for the investigated metals due to their differences in mass fraction profiles. Therefore, we cannot expect that the abundance ratios determined by Gibson et al. (2022) ([Fe/Mg], [V/Ti], [Fe/Cr], [Fe/V], and [Fe/Ti] seen in Figure 4.15) are reliably estimated. This is

especially true considering the large values of χ^2_{red} found for Fe, as seen in section 4.2. The discrepancy between HK17's approximation and `petitRADTRANS` was largest for Fe, and it is problematic to constrain relative abundances with other species at such high temperatures. The main point of their study was to demonstrate their framework using UVES transmission spectroscopy of WASP-121b to constrain temperature-pressure profiles and, most importantly, relative abundances.

The choice of species to perform retrievals on by Gibson et al. (2022) would likely have ended up pretty accurate if the planetary temperature was around 1500 K. However, WASP-121b is one of the hottest known exoplanets, and in Gibson et al. (2022) they constrained a temperature of $\approx 3140 \pm 290$ K in the upper atmosphere. According to our results, the HK17 approximation yields weaker lines for these temperatures than `petitRADTRANS` and the constraints on relative abundances found by Gibson et al. (2022) might be underestimated. However, it is worth noting that in their study, they used a temperature-pressure profile by Guillot (2010). Using this temperature-pressure profile would be a future prospect of this project, but it was not investigated as time did not permit it.

As mentioned briefly in section 4.1, we can only use one opacity function in the analytical approximation by HK17. As `petitRADTRANS` interpolates the opacity function for the investigated species for each atmospheric layer of pressure, we get pressure broadening. The best choice of opacity function in HK17 was at a pressure of 1 mbar. We did investigate opacity functions for other pressures, but ultimately they did not perform as well as the one for 1 mbar.

Ideally, there would be a way to include multiple opacity functions in the HK17 approximation, as well as varying chemical abundances, a MMW dependent on pressure, and a variable gravity. An attempt was made to expand the HK17 approximation to include variable gravity by including a gravity dependent on altitude in the scale height, such that

$$H = \frac{kT}{mg(r)}. \tag{4.2}$$

However, by doing so, we end up with an integral later in the derivation of the transit radius, which was beyond the scope of the project to solve.

Although our results show a discrepancy between the HK17 solution and `petitRADTRANS`, especially at high temperatures, we acknowledge that the analytical approximation is much faster and that a fast model is necessary for retrievals. This is especially true when we wish to create tens or hundreds of thousands of model templates, as they did in Gibson et al. (2022).

Chapter 5

Conclusions

We have analysed eight different species of molecules, atoms, and ions, at temperatures of 1500 K, 2500 K, and 3500 K, using the planetary parameters of the hot Jupiter HD 209458b. The correlation between transmission spectra computed by the HK17 approximation and `petitRADTRANS` is strong for H_2O at 1500 K up to 2500 K. At higher temperatures, the approximation overestimates the spectral line strengths and can no longer be reliably used.

When modelling the transmission spectra of Fe II for 2500 K and 3500 K, we conclude that it is not advisable to use the HK17 approximation for abundance retrievals of species whose mass fraction increases with altitude. We cannot find a representable value for the mass fraction which means that the HK17 solution will either underestimate or overestimate the spectral lines. The appearance of the spectral lines when using variable mass fractions occurs rapidly between temperatures of 2500 K and 3500 K. For abundance retrievals, this means that the planet's temperature must be chosen carefully to retrieve an accurate transmission spectrum. Furthermore, we conclude that Fe II is highly sensitive to the varying abundance, variable gravity, and pressure broadening throughout the atmosphere.

For the other species (CO, Fe, Ti, V, Mg, and Cr), we find that the correlation between the `petitRADTRANS` solution and HK17's approximation does poorly to different degrees, and the metals cannot be used for abundance ratio retrievals. Therefore, we conclude that Gibson et al. (2022)'s results are not reliably estimated, considering the discrepancies between species. For such retrievals, we do see the need for fast models when hundreds of thousands of model templates are necessary. However, considering that WASP-121b is an ultra-hot Jupiter and we see the larger discrepancies between the solutions by `petitRADTRANS` and HK17 at high temperatures, it is inadvisable to use the approximation for retrievals of ultra-hot Jupiters.

By only including one opacity function in the HK17 approximation, we neglect pressure broadening, which shapes the appearance of a transmission spectrum. To produce a transmission spectrum that takes as many physical processes into account as possible, many opacity functions must be used throughout the atmosphere. It is also necessary to include atmospheric chemistry, as most mass fractions and the MMW span many orders of magnitude throughout the atmospheric layers. We have seen that variable gravity has a huge impact on the transmission spectrum and inflates the scale height, conclud-

ing that the use of constant gravity yields worse results as we reach high temperatures. Finally, approximating the atmosphere to be isothermal is not physically realistic. We need to adopt a non-isothermal temperature-pressure profile since this would result in, for instance, different mass fractions and MMW.

Overall, the HK17 approximation performs well for most species at 1500 K, though we have to be careful when using it to ensure that our application of the approximation fits within the scope of its capabilities. For example, it does well when producing a transmission spectrum of H_2O for a temperature less than 2500 K. However, it is unreliable when we have a mass fraction which increases with altitude or wish to perform abundance retrievals of ultra-hot Jupiters.

5.1 Future prospects

Although our understanding of the performance of HK17's approximation at high spectral resolution has developed from the project, many questions are still left unanswered. First, if the project was expanded upon, we would like to explore non-isothermal atmospheres through the temperature-pressure profile from Guillot (2010). Secondly, we did not manage to include variable gravity in the HK17 formula, but that does not mean that it is impossible. Furthermore, the inclusion of chemistry with variable mass fractions and MMW has an important role in computing the transmission spectrum. It should be investigated whether these could be introduced for the HK17 approximation.

The approximation also needs to be tested for other planetary parameters. However, this project aimed to test its performance using the parameters of the hot Jupiter HD 209458b, as this was the object of HK17's analysis. Lastly, the HK17 approximation assumes that the atmosphere is isobaric, which means that there is no pressure broadening. However, to include pressure broadening, and all the aforementioned implementations, would stray the HK17 formula further from an approximation and could increase the computational time. Though this would improve its accuracy, a balance is necessary for approximations to remain fast enough for retrieval algorithms.

Bibliography

Andrae, R., Schulze-Hartung, T., & Melchior, P. 2010, Dos and don'ts of reduced chi-squared

Asplund, M., Grevesse, N., Sauval, A. J., & Scott, P. 2009, ARA&A, 47, 481

Atkins, P. W. & De Paula, J. 2006, Atkins' Physical Chemistry (New York: W.H. Freeman)

Batalha, N. M. 2014, Proceedings of the National Academy of Sciences, 111, 12647

Boley, A. C., Laerhoven, C. V., & Contreras, A. P. G. 2020, The Astronomical Journal, 159, 207

Borucki, W. J., Koch, D., Basri, G., et al. 2010, Science, 327, 977

Brogi, M., Line, M., Bean, J., Désert, J.-M., & Schwarz, H. 2017, ApJ, 839, L2

Cessa, V. 2019, in International Conference on Space Optics — ICSO 2018, Vol. 11180, International Society for Optics and Photonics (SPIE), 1363 – 1363

Chandrasekhar, S. 1960, Radiative transfer (New York: Dover)

Deeg, H. J. & Alonso, R. 2018, Handbook of Exoplanets, 633–657

Deljookorani, S., Kunzle, V., & Leger, D. 2020, Journal of Research in Progress, 3, 57

Deming, D., Wilkins, A., McCullough, P., et al. 2013a, ApJ, 774, 95

Deming, D., Wilkins, A., McCullough, P., et al. 2013b, ApJ, 774, 95

Dressel, L. 2021, Wide Field Camera 3 Instrument Handbook, Version 13.0 ((Baltimore: STScI))

Flowers, E., Brogi, M., Rauscher, E., Kempton, E. M.-R., & Chiavassa, A. 2019, The Astronomical Journal, 157, 209

Fortney, J. J., Dawson, R. I., & Komacek, T. D. 2021, Journal of Geophysical Research: Planets, 126

Fortney, J. J., Lodders, K., Marley, M. S., & Freedman, R. S. 2008, The Astrophysical Journal, 678, 1419

Fortney, J. J., Shabram, M., Showman, A. P., et al. 2010, ApJ, 709, 1396

Gibson, N. P., Merritt, S., Nugroho, S. K., et al. 2020, Monthly Notices of the Royal Astronomical Society, 493, 2215

Gibson, N. P., Nugroho, S. K., Lothringer, J., Maguire, C., & Sing, D. K. 2022, MNRAS, 512, 4618

Grimm, S. L., Malik, M., Kitzmann, D., et al. 2021, , 253, 30

Guillot, T. 2010, A&A, 520, A27

Heng, K. & Kitzmann, D. 2017, Monthly Notices of the Royal Astronomical Society, 470, 2972–2981

Howell, S. B. 2020, Frontiers in Astronomy and Space Sciences, 7, 10

Kitzmann, D., Heng, K., Rimmer, P. B., et al. 2018, The Astrophysical Journal, 863, 183

Krupenie, P. 1966, The Band Spectrum of Carbon Monoxide, NSRDS-NBS (U.S. Department of Commerce, National Bureau of Standards)

Line, M. R., Knutson, H., Deming, D., Wilkins, A., & Desert, J.-M. 2013, The Astrophysical Journal, 778, 183

Lothringer, J. D. & Barman, T. 2019, The Astrophysical Journal, 876, 69

Madhusudhan, N. 2012, ApJ, 758, 36

Mayor, M., Pepe, F., Queloz, D., et al. 2003, The Messenger, 114, 20

Mayor, M. & Queloz, D. 1995, Nature, 378, 355

Merritt, S. R., Gibson, N. P., Nugroho, S. K., et al. 2020, A&A, 636, A117

Mollière, P., Stolker, T., Lacour, S., et al. 2020, Astronomy and Astrophysics, 640

Mollière, P., Wardenier, J. P., van Boekel, R., et al. 2019, Astronomy Astrophysics, 627, A67

Pearson, K. 1900, The London, Edinburgh, and Dublin Philosophical Magazine and Journal of Science, 50, 157

Pepe, F., Cristiani, S., Rebolo, R., et al. 2021, A&A, 645, A96

Ricker, G. R., Vanderspek, R., Winn, J., et al. 2016, in Space Telescopes and Instrumentation 2016: Optical, Infrared, and Millimeter Wave, Vol. 9904, International Society for Optics and Photonics (SPIE), 767 – 784

Robinson, T. & Catling, D. 2013, Nature Geoscience, 7

Showman, A. P., Tan, X., & Parmentier, V. 2020, Space Science Reviews, 216, 139

Spiegel, D. S., Fortney, J. J., & Sotin, C. 2014, Proceedings of the National Academy of Sciences, 111, 12622

Spiegel, D. S., Silverio, K., & Burrows, A. 2009, The Astrophysical Journal, 699, 1487

Stock, J. W., Kitzmann, D., Patzer, A. B. C., & Sedlmayr, E. 2018, Monthly Notices of the Royal Astronomical Society

Swain, M. R., Estrela, R., Roudier, G. M., et al. 2021, The Astronomical Journal, 161, 213

Winn, J. N. 2014, Transits and Occultations

Wolszczan, A. & Frail, D. 1992, Nature, 355, 145–147

Yan, F., Pallé, E., Reiners, A., et al. 2020, A&A, 640, L5